Title

Intracellular mechanosensation in intestinal smooth muscle: Piezo1 complexes amplify signalling beyond the surface

Journal

The Journal of Physiology

ISSN

0022-3751

Authors

Bautista, Geoanna M

Manning, Declan

Lieu, Emily C

et al.

Publication Date

2026-09-10

DOI

10.1113/jp291215

The Journal of Physiology

Intracellular mechanosensation in intestinal smooth muscle: Piezo1 complexes amplify signalling beyond the surface

Geoanna M. Bautista[1], Declan Manning[2], Emily C. Lieu[1], Stephanie I. Ugochukwu[1], Collin Matsumoto[2], Joshua P. Tulman[2], Miguel Martin-Aragon Baudel[3], Nuria Daghbouche-Rubio[3], Steven J. McElroy[1], Sal A. Baker[4], Manuel F. Navedo[3] and L. Fernando Santana[2]

[1]*Department of Pediatrics, University of California Davis, Sacramento, California, USA*
[2]*Department of Physiology and Membrane Biology, University of California Davis, Davis, California, USA*
[3]*Department of Pharmacology, University of California Davis, Davis, California, USA*
[4]*Department of Physiology, University of Nevada Reno, Reno, Nevada, USA*

Handling Editors: Peying Fong & Jonathan Silva

The peer review history is available in the Supporting Information section of this article (https://doi.org/10.1113/JP291215#support-information-section).

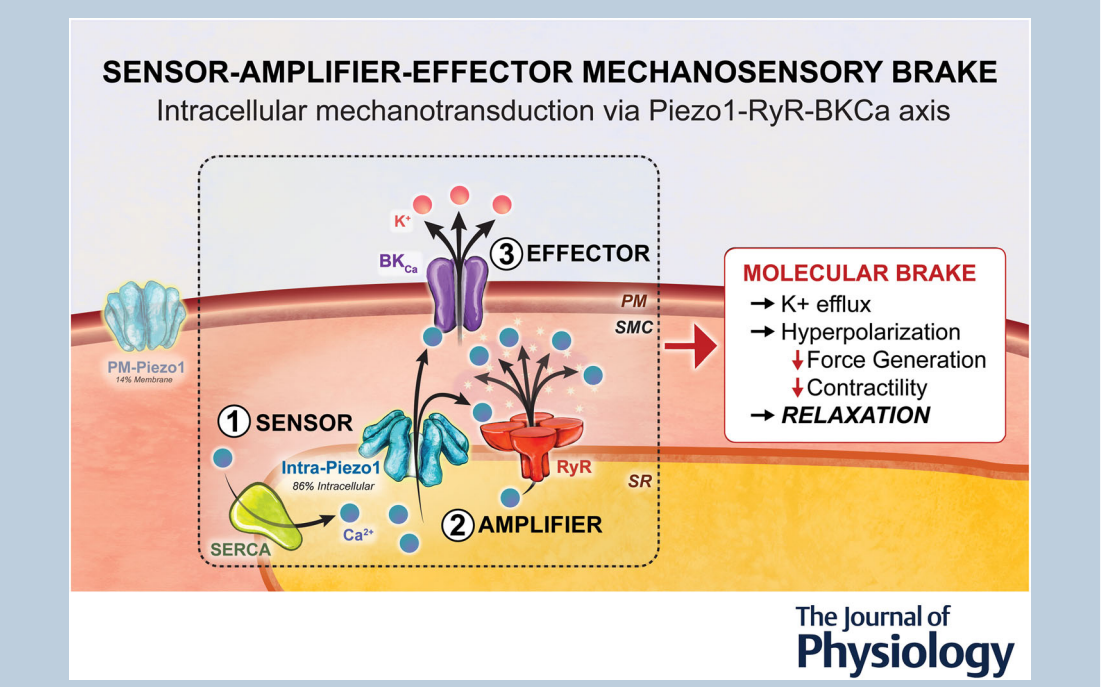

Abstract figure legend Mechanosensation is not confined to the cell surface. In intestinal smooth muscle Piezo1 is predominantly intracellular (86%), where it forms a nanoscale (<40 nm) complex at the sarcoplasmic reticulum (SR)–plasma membrane junction. Within this sensor–amplifier–effector axis intra-Piezo1 is the sensor that detects force at the SR, ryanodine receptor (RyR) is the amplifier that converts it into Ca^{2+} release and BK_{Ca} is the effector that

The content is solely the responsibility of the authors and does not necessarily represent the official views of the University of California, Davis. This article was first published as a preprint. Bautista GM, Manning D, Lieu EC, Matsumoto C, Ugochukwu SI, Tulman JP, Martin-Aragon Baudel M, Daghbouche-Rubio N, McElroy SJ, Baker SA, Navedo MF, Santana LF. 2026. Intracellular mechanosensation in intestinal smooth muscle: Piezo1 complexes amplify signaling beyond the surface. bioRxiv. https://doi.org/10.64898/2026.02.19.706403.

DOI: 10.1113/JP291215

translates Ca^{2+} into K^+ efflux and membrane hyperpolarization. The result is reduced contractility, Piezo1 acting as a molecular brake that restrains smooth muscle excitability and tunes gastrointestinal motility.

Abstract Mechanosensation is fundamentally viewed as a plasma membrane phenomenon. We challenge this paradigm by introducing intracellular mechanosensation in intestinal smooth muscle. We hypothesized that a distinct, organelle-based signalling axis exists to amplify mechanotransduction from the inside out. To test this we investigated whether Piezo1, a canonical plasma membrane (PM) mechanosensor, also operates within the cell. Using tissue-level wire myography, high-resolution confocal microscopy, proximity ligation assays and patch-clamp electrophysiology on freshly dissociated cells, we identified a previously uncharacterized Piezo1-RyR-BK_{Ca} signalling axis in small intestinal smooth muscle cells (SMC). This intracellular mechanism relies on a nanoscale signalling complex (<40 nm) comprising an intracellular sensor (intra-Piezo1) and an amplifier (ryanodine receptor, RyR), coupled with a PM effector (large-conductance, Ca^{2+}-activated K^+ channels, i.e., BK_{Ca} channels). Activating this intracellular complex generated paxilline-sensitive outward currents independent of extracellular Ca^{2+} and dependent on internal SR Ca^{2+} stores, consistent with intrinsic organellar mechanotransduction. Within this complex intra-Piezo1 and RyR are positioned to operate as a coupled SR Ca^{2+} release unit that activates BK channels at SR–PM junctions, driving potent membrane hyperpolarization that reduces smooth muscle contractility, revealing the intra-Piezo1 complex as a molecular brake on excitation. These findings support a model in which mechanotransduction is not confined to the cell surface. Instead a specialized sensor–amplifier–effector complex originating at intracellular organelles amplifies cellular sensitivity to physical force, providing a critical gain-control system that restrains smooth muscle excitability and regulates gastrointestinal (GI) motility.

(Received 23 February 2026; accepted after revision 29 July 2026; first published online 10 September 2026)
Corresponding author G. M. Bautista: Department of Pediatrics, University of California Davis, Sacramento, CA, USA. Email: gmbautista@health.ucdavis.edu

Key points

- This study advances a framework in which intracellular organelles contribute to mechanosensory signalling in gastrointestinal (GI) smooth muscle cells, complementing plasma membrane mechanisms.
- Piezo1 is predominantly intracellular in intestinal smooth muscle, where this pool, intra-Piezo1, forms a nanoscale signalling complex on the sarcoplasmic reticulum (SR) that positions it within <40 nm of RyR and of sarcolemmal large-conductance, Ca^{2+}-activated K^+ (BK_{Ca}) channels.
- Electrophysiological recordings show that this 'sensor–amplifier–effector' mechanism generates potent paxilline-sensitive hyperpolarizing currents that depend on SR Ca^{2+} release and persist without extracellular Ca^{2+}, amplifying the cell's response to mechanical stress when intra-Piezo1 is activated from the inside out.
- Activation of this intra-Piezo1-mediated axis significantly dampens smooth muscle contractility, acting as a molecular 'brake' that supports the stretch-induced-relaxation feedback mechanism essential for intestinal function.

Introduction

Mechanotransduction is a fundamental physiological process by which cells convert physical forces, such as shear stress, tension and hydrostatic pressure, into biochemical signals (Huang et al., 2004). This conversion is essential for diverse biological functions, ranging from vascular tone regulation to sensory perception. In smooth muscle mechanical stimuli such as intraluminal pressure or tissue stretch trigger changes in intracellular Ca^{2+} that regulate contractility and gene expression (Hill-Eubanks et al., 2011). However Ca^{2+} signalling in mechanotransduction involves considerable

spatiotemporal complexity rather than simple global changes (Earley, 2013).

In the gastrointestinal (GI) tract mechanosensitivity is essential for co-ordinating motor patterns that drive peristalsis, regulate luminal flow and maintain barrier function (Mercado-Perez & Beyder, 2022). The intestinal wall undergoes continuous mechanical activity from luminal distension, peristaltic strain and fluid shear stress. The intestinal smooth muscles must then integrate these diverse mechanical signals through the SIP syncytium, an electrically coupled network that includes interstitial cells of Cajal and Pdgfrα^+ cells (Sanders, 2019; Sanders et al., 2023), to collectively drive the motor patterns required for intestinal homoeostasis.

Central to this process are mechanosensitive ion channels (MSCs), which rapidly gate in response to membrane deformation and convert mechanical forces into electrical signals across diverse physiological systems (Alcaino et al., 2017; Gu & Gu, 2014). In GI smooth muscle these consist of Piezo1 channels and transient receptor potential (TRP) channels, which contribute to depolarizing cation currents, potassium channels like Ca^{2+}-activated K^+ channels (BK_{Ca}) and TREK-1 that provide negative feedback to reduce overexcitability (Alcaino et al., 2017; Berrier et al., 2013; Gonzalez-Cobos & Trebak, 2010; Sanders & Koh, 2006). These channels have been predominantly studied and understood as plasma membrane mechanosensors, positioned to detect extracellular mechanical forces and translate them into electrical and Ca^{2+} signals that regulate contractility via interactions with nearby voltage-gated Na^+ and Ca^{2+} channels (Sanders, 2008).

This plasma membrane (PM)-centric paradigm underpins current mechanotransduction models in GI smooth muscle. According to this framework Piezo1 channel activation at the PM would lead to cation influx, membrane depolarization and the activation of voltage-gated Ca^{2+} channels ($Ca_V1.2$) (Joshi et al., 2021). This sequence is traditionally viewed as an excitatory cascade: Force → Cation Influx → Contraction, a model supported by data in vascular tissues where Piezo1 activation clearly modulates Ca^{2+}-dependent excitation (Lim & Harraz, 2024).

However Piezo1$^{-/-}$ intestinal smooth muscle presents a striking paradox. Rather than simply losing mechanosensitive excitation these tissues exhibit profound compensatory remodelling: upregulation of Ano1 Ca^{2+}-activated Cl^- channels and increased $Ca_V1.2$ expression drive electrical hyperexcitability, yet contractile force remains significantly reduced compared to wild type (Bautista et al., 2025). This dissociation of enhanced excitation coupled with diminished contraction cannot be simply explained by the loss of a plasma membrane excitatory channel. If Piezo1 deletion merely removed one source of depolarizing current, compensatory upregulation of other excitatory channels should restore or even enhance contractility. Instead the tissue becomes more electrically excitable, but contractions become even weaker. Piezo1 deletion therefore appears to remove a mechanosensory signal that is not simply excitatory, implying a more complex role (Bautista et al., 2025, 2026)

A new body of evidence is challenging the previous paradigm that mechanotransduction is restricted to the cell surface. Early studies identified Piezo1 in the endoplasmic reticulum (ER) of epithelial cells (McHugh et al., 2010) and showed that the channel is bound and suppressed by the sarcoplasmic reticulum (SR)/ER Ca^{2+}-ATPase SERCA2, placing an SR-resident protein in direct physical contact with Piezo1 (Zhang et al., 2017). More recently Liao et al. (2021) provided evidence for intracellular Piezo1 in pulmonary smooth muscle, where it mediates Ca^{2+} release from the SR independently of extracellular Ca^{2+}. These findings point towards a concept of 'intracellular mechanosensation', in which organelles possess intrinsic capabilities to detect and respond to physical stress. Based on these emerging data and the functional deficits reported by our group (Bautista et al., 2025) we hypothesized that the primary role of Piezo1 in GI smooth muscle is not to mediate surface influx but to anchor a specialized intracellular signalling complex. We propose that this complex localizes to the SR and functionally couples the mechanosensor (Piezo1) to intracellular amplification machinery (ryanodine receptors (RyR) and BK channels).

To test this hypothesis we used high-resolution confocal microscopy and proximity ligation assays (PLA) to map the nanoscale architecture of Piezo1 relative to SR calcium release channels in intestinal smooth muscle. We combined these approaches with patch-clamp

Geoanna Marie Bautista is an assistant professor of paediatrics in the Division of Neonatology at the University of California, Davis Children's Hospital. As a neonatologist and physician-scientist she leads a basic and translational research programme investigating how mechanical forces regulate intestinal motility and inflammation. By examining the consequences of disrupting these tightly regulated pathways her laboratory aims to elucidate the precise signalling mechanisms driving normal *versus* maladaptive development of the neonatal gut. Ultimately Dr. Bautista seeks to bridge these mechanistic discoveries with clinical advancements in neonatal care while actively mentoring the next generation of physician-scientists.

electrophysiology and wire myography to determine whether activating this complex drives hyperpolarizing currents dependent on internal stores rather than surface entry, thereby altering contractile properties. Our data support an 'intracellular mechanosensation' pathway in which organelle-based Piezo1 complexes amplify mechanotransduction to fine-tune GI motility.

Materials and methods

Ethical approval

All animal procedures were approved by the University of California, Davis Institutional Animal Care and Use Committee (IACUC Protocol #25185), and conducted in accordance with the National Institutes of Health Guide for the Care and Use of Laboratory Animals. Adult male and female C57BL/6J mice (8–12 weeks old, 20–30 g body weight; RRID: IMSR_JAX:000664) were obtained from Jackson Laboratory (Bar Harbor, ME, USA) and housed under standard laboratory conditions (12:12 h light–dark cycle, 22 ± 2°C, *ad libitum* access to standard rodent chow and water). For immunocytochemistry experiments, Piezo1-tdTomato reporter mice (Piezo1$^{tm1.1Apat}$, Jackson Laboratory, Bar Harbor, ME, USA; Stock #02 9214; RRID: IMSR_JAX:02 9214) were bred and maintained as described previously (Ranade et al., 2014). Both male and female mice were used as indicated, and data were pooled because no sex × treatment interaction reached significance for any parameter (Tables A1, A6); sex main effects on peak contraction and relaxation velocity are reported in Table A1 and addressed in the Discussion section. Mice were killed by isoflurane inhalation (5% in O_2) followed by cervical dislocation. Death was confirmed by the absence of heartbeat and toe-pinch reflex.

Tissue preparation and cell dissociation

After euthanasia the small intestine was rapidly excised and placed in ice-cold (4°C) Ca^{2+}-free physiological buffered solution (PBS) or modified Hank's solution (MHS) containing (in mM): 125 NaCl, 5.36 KCl, 2 $MgCl_2$, 0.336 Na_2HPO_4, 0.44 K_2HPO_4, 11 HEPES, 15.5 $NaHCO_3$, 10 Glucose and 2.9 sucrose, pH 7.4. External muscularis layers were peeled and gently separated from the mucosa and then equilibrated in Ca^{2+}-free MHS. Freshly dissociated smooth muscle cells (SMCs) were obtained for patch-clamp electrophysiology, immunocytochemistry (ICC) and PLA, as described previously (Koh et al., 1998). Briefly muscle strips were incubated in two successive Ca^{2+}-free enzyme solutions containing (per ml): 1) papain (Thermo Fisher, 0.5-1 mg), DTT (Sigma, 1 mg), bovine serum albumin (Sigma, 1 mg) and 2) collagenase (Worthington, Type II, 2 mg), trypsin inhibitor (Worthington, 1 mg), bovine serum albumin (BSA) (Sigma, 2 mg) and ATP (Sigma, 0.27 mg).

Wire myography

Tissue equilibration. Segments of murine small intestine (full-thickness and peeled muscularis, approximately 3 mm in length) were mounted on a wire myograph (DMT820MO, Danish Myo Technology, Denmark) in Krebs-Ringer bicarbonate solution maintained at 37°C and pH 7.40, continuously bubbled with carbogen (95% O_2/5% CO_2). After mounting preparations were allowed to equilibrate for 30 min with solution changes every 10 min. Spontaneous contractile activity was recorded continuously using LabChart software (AD Instruments, Colorado Springs, CO, USA) at a sampling rate of 250 Hz. Force data were exported as tab-delimited text files for offline analysis.

Experimental protocols. After stable spontaneous contractions were established for 5 min (steady-state baseline), pharmacological agents were added cumulatively to the organ bath. For Piezo1 activation experiments Yoda2 (Sigma-Aldrich, St. Louis, MO, USA (DTT, BSA, ATP, glycine, glyoxal, Yoda2, Duolink reagents), 25 μM) was applied, and responses were recorded for 30 min. Yoda2, a second-generation Piezo1 activator with improved selectivity and potency compared to Yoda1, was chosen for its advantages in *ex vivo* tissue preparations and consistent activation across cell-permeable compartments. For RyR experiments tissue was pretreated with ryanodine (ABCAM, Cambridge, UK (Ryanodine), 100 μM) for 60 min prior to Yoda2 application. For SR Ca^{2+} store depletion experiments tissue was pretreated with Thapsigargin (Fisher, 10 μM) for 15 min prior to Yoda2 application. Vehicle controls (0.1% DMSO) showed no significant effects on contractile parameters.

Contractile analysis. Contractile force recordings were analysed using a custom Python-based analysis toolkit (source code available at https://doi.org/10.5281/zenodo.18472624). Raw force traces were imported and processed to detect contractions using automated peak detection (Wire Myography Analyzer v_4; SciPy find_peaks) with validated settings: prominence and height thresholds set at 0.05 mN, a minimum interpeak distance of 1.0 s and a minimum peak width of 0.3 s. Metrics such as frequency (cpm), amplitude (mN) and kinetic parameters (rise/relaxation rates) were derived from standardized 150 s analysis windows. Technical replicates from the same animal were averaged for statistical analyses. Contractile parameters were compared before and after drug application using paired comparisons within the same tissue preparation. Therefore variability due to tissue

size is inherently controlled for within each paired analysis, and normalization to cross-sectional area was not required and would not necessarily improve the variability (Erdogan et al., 2020). Validation plots were generated for each recording, showing the trace with marked peaks, the calculated baseline and the detection threshold. All plots were visually inspected to confirm accurate peak detection. Recordings with substantial movement artifacts, unstable baselines or equipment issues were excluded from analysis.

Whole-cell patch-clamp electrophysiology

Recording configuration. Whole-cell voltage-clamp recordings were obtained from freshly isolated intestinal SMCs at room temperature using an Axopatch 200B amplifier, a Digidata 1440 digitizer and Clampex 10 software; data were analysed using Clampfit (Molecular Devices, Sunnyvale, CA, USA). Borosilicate glass pipettes (P-97 puller, Sutter Instruments, Novato, CA, USA) were polished to a resistance of 2–4 MΩ. Cells were voltage-clamped at a holding potential of −50 mV; currents were sampled at 50 kHz and low-pass filtered at 2 kHz; recordings were acquired in gap-free mode.

Solutions. Standard external Tyrode's III solution contained (in mM) the following: 140.0 NaCl, 5.4 KCl, 1.8 $CaCl_2$, 1.0 $MgCl_2$, 5.0 HEPES and 5.5 glucose, adjusted to pH 7.4 with NaOH. The internal pipette solution contained (in mM) the following: 5.0 NaCl, 140.0 KCl, 10.0 HEPES, 5.0 MgATP and 10.0 EGTA, adjusted to pH 7.2 with NaOH.

Experimental protocols. Freshly dissociated SMCs were allowed to settle on glass coverslips for at least 5 min before recording. After the whole-cell configuration was achieved, SMCs were held at −50 mV and dialyzed with internal solution for at least 2 min before starting protocols. Solution changes were achieved using a gravity-fed perfusion system. Patch-clamp experiments were performed at room temperature (22°C–24°C).

Yoda2 protocols: for agonist-only experiments a 30 s baseline was recorded in 1.8 mM Ca^{2+} Tyrode's III followed by 90 s of Yoda2 (10 μM) in 1.8 mM Ca^{2+} Tyrode's III and then washout with drug-free 1.8 mM Ca^{2+} Tyrode's III. For Yoda2 plus paxilline experiments a 30 s baseline was followed by 90 s of Yoda2 (10 μM), 90 s of Yoda2 plus paxilline (10 μM) and then washout with 1.8 mM Ca^{2+} Tyrode's III.

Thapsigargin protocol: for thapsigargin (TG) experiments intestinal SMCs (ISMCs) were preincubated for 20 min in 1.8 mM Ca^{2+} Tyrode's III containing TG (1 μM) and allowed to adhere to glass coverslips. After whole-cell configuration was established at −50 mV, cells were continuously perfused with 1.8 mM Ca^{2+} Tyrode's III containing 1 μM TG; after a 30 s baseline perfusion was switched to the same solution containing Yoda2 (10 μM) for 90 s and then returned to TG-only solution for a 30 s washout.

Acute Ca^{2+} removal protocol: to examine acute extracellular Ca^{2+} removal a 30 s baseline was recorded in 1.8 mM Ca^{2+} Tyrode's III. The solution was then switched to Ca^{2+}-free Tyrode's III for 30 s. Cells were perfused for 90 s with 0 mM Ca^{2+} Tyrode's III containing Yoda2 (10 μM), then for 90 s with Yoda2 plus paxilline (10 μM), followed by a Ca^{2+}-free washout and finally re-exposure to 1.8 mM Ca^{2+} Tyrode's III for 30 s.

Analysis. Patch-clamp data were exported using Clampfit software (Molecular Devices) and analysed in Microsoft (Redmond, WA, USA) Excel. Means to describe various drug conditions were obtained by averaging pA values during the last 10 s of the baseline, TG and paxilline conditions. For the Yoda2 protocols pA values at the peak of the response were recorded and normalized to the cell capacitance to account for physiological variation across cell sizes. Averaged values reflect the peak current within each epoch rather than an epoch average. The 90 s analysis window was chosen to standardize measurements across all preparations and conditions based on the consistent plateau observed starting at 90 s and lasting up to 120 s in preliminary experiments.

Immunocytochemistry/immunofluorescence

Immunostaining. SMCs were fixed in 4% paraformaldehyde, quenched with 50 mM glycine and stained with Alexa Fluor 488-conjugated wheat germ agglutinin (WGA; 5 μg/mL). Cells were blocked in 3% BSA and 0.25% Triton X-100 before overnight incubation with anti-RyR2 (1:50) and anti-RFP (1:100). Secondary antibodies included 568-conjugated goat anti-chicken IgY and Cy5-conjugated goat anti-mouse IgG. Images were captured using a Dragonfly 200 spinning disc confocal (Andor) through a 60× oil immersion objective (NA 1.40). Z-stacks were acquired with 178 nm separation and processed using three-dimensional (3-D) deconvolution.

Imaging acquisition. Immunofluorescence images were captured using a Dragonfly 200 spinning disc confocal (Andor) through a DMi* Leica microscope (Leica) equipped with a 60× oil immersion objective (NA 1.40) and Andor iXon EMCCD cameras. Laser lines at 488, 561 and 637 nm were used to specifically excite WGA-488, RFP/Alexa Fluor-568 and Alexa Fluor-647, respectively. Image acquisition was conducted using Fusion software (Andor) to capture z-stacks with a separation of 178 nm

between image slices and apply 3-D deconvolution to image stacks.

Immunofluorescence image analysis. Image stacks were segmented using Imaris 10.2.0 software (Oxford Instruments, Zurich, Switzerland). WGA-488 signal was traced manually to delineate the plasma membrane using the Surfaces tool. RyR and Piezo1-associated fluorescence signals were mapped to *x*/*y*/*z* centroid co-ordinates using the Spots tool, assigning Spots to any fluorescence signals exceeding a fixed threshold with a diameter exceeding 120 nm in all dimensions. 'Region Growing' was then applied to assign variable sizes to Spots, determined by the size and brightness of their corresponding fluorescent puncta. Spots were assigned to plasma membrane-associated (Membrane) and non-membrane-associated (Internal) groups, delimited by a 200 nm distance between the centroid *x*/*y*/*z* position of the Spots and the plasma membrane Surface, and colocalization of Piezo1 with RyR clusters was determined by a 240 nm centroid co-ordinate proximity cut-off.

Proximity ligation assay

PLAs were performed using the Duolink PLA system as described previously (Martín-Aragón Baudel et al., 2022); Sigma, #DUO92008) to detect Piezo1-containing complexes with either RyR or BKα subunits. Freshly dissociated SMCs were plated onto glass coverslips and allowed to adhere. Cells were fixed in glyoxal solution (Sigma–Aldrich, #128 465) for 20 min, washed in PBS and quenched with 100 mM glycine (Sigma–Aldrich, #50 046) in PBS for 15 min, followed by two additional 5 min washes in PBS. Cells were permeabilized with 0.1% Triton X-100 for 20 min and blocked in 20% Blocking Buffer (LI-COR Biosciences, #927-60 001) for 1 h at 37°C. Cells were incubated overnight at 4°C with primary antibodies against Piezo1 (rabbit anti-Piezo1; Alomone Labs, Jerusalem, Israel, APC-087, 1:200) in combination with either mouse anti-RyR2 (Invitrogen C3-33, 1:200) or mouse anti-BKα (NeuroMab, Antibodies Incorporated, Davis, CA, USA, clone L6/60, 1:200). PLA detection was performed using Duolink rabbit PLUS and mouse MINUS probes (1:5 dilution in Duolink Antibody Diluent) for 1 h at 37°C. Cells were washed thrice for 5 min in Duolink Buffer A and incubated with ligation solution for 30 min at 37°C to allow hybridization and circular DNA template formation at sites of dual labelling. After three additional 3 min washes in Buffer A cells were incubated with the amplification solution for 120 min at 37°C. Coverslips were then washed twice for 10 min in Duolink Buffer B, 1 min in 1% Buffer B, air-dried and then mounted using Duolink mounting medium (#DUO82040).

PLA signals were imaged using an Olympus (Tokyo, Japan) Fluoview FV3000 confocal microscope equipped with a 60× oil-immersion objective (NA 1.42) and OBIS 405- and 561 nm lasers, controlled using Olympus (Tokyo, Japan) 31S-SW software. Confocal z-stacks were acquired at 0.5 µm step size using constant acquisition settings across conditions. Maximum-intensity projections were generated using Fiji (version 2.17.0). PLA puncta were quantified in the 561 nm channel using a custom Fiji macro with a fixed threshold applied uniformly across all images. PLA image stacks were then segmented using Imaris 10.2.0 software (Oxford Instruments). Brightfield transmitted light was traced manually to delineate the plasma membrane using the Surfaces tool, and puncta were mapped to *x*/*y*/*z* centroid co-ordinates using the Spots tool, capturing fluorescence signals exceeding a fixed threshold and with diameters exceeding 500 nm in all dimensions. Membrane-associated and internal PLA puncta were discriminated using a 1 µm cut-off distance to the plasma membrane surface. Intranuclear puncta were excluded from all analyses. For quantitative group comparisons individual cell measurements were aggregated into per-animal means to control for inter-animal variability.

Statistical analysis

Data are presented as mean ± SD. Normality was assessed using the Shapiro-Wilk test. Parameters that met normality were analysed using repeated-measures one-way ANOVA with Geisser-Greenhouse correction and Holm–Šídák *post hoc* tests (Tables A3 and A4) or Bonferroni *post hoc* tests (Table A5), as indicated in each table. Parameters that did not meet normality, namely frequency in the GsMTx4 series, integral force and frequency in the Jedi2 series and amplitude in the ryanodine series, were analysed using the Friedman test and Dunn's *post hoc* test (Tables A3 and A4). Paired comparisons within the same preparation or cell were analysed using paired *t* tests. To account for pseudo replication technical replicates were averaged within each animal before statistical comparison, ensuring biological variation (N = animals) determined statistical power. Sample sizes are reported as n (cells/segments/preparations) from N (animals). For immunocytochemistry per-cell measurements were averaged within each animal, and compartment comparisons were made using paired *t* test on those per-animal means (N = 10 mice); sex was assessed by comparing the plasma membrane value between sexes (N = 5 males *vs.* 5 females), using an unpaired *t* test with Welch's correction, or the Mann–Whitney test where the Shapiro-Wilk normality test was not met within a sex. Descriptive statistics for these panels are reported

Table 1. Steady-state contractile parameters of Yoda2 induced Piezo1 activation

Parameter	Fig. 1*D*	Baseline	Yoda2	%	*t*(11)	*P*-value	Cohen's *d*
Amplitude (mN)	i	0.2976 ± 0.1082	0.1276 ± 0.0433	−57	7.393	1.37×10^{-5}	2.1343
Integral force (mN·s)	ii	17.8625 ± 5.5282	7.7758 ± 2.7442	−56	9.488	1.25×10^{-6}	2.7389
Frequency (cpm)	iii	31.6675 ± 3.4938	28.6840 ± 5.8413	−9	2.393	0.0357	0.6908
Period CV (%)	iv	9.6938 ± 5.9387	24.4586 ± 15.5017	152	−3.092	0.0103	0.8926
Duration (s)	v	1.5540 ± 0.1967	1.7168 ± 0.1773	10	−3.106	0.0100	0.8966
d*F*/d*t* max (mN/s)	vi	3.4513 ± 0.7009	2.9626 ± 0.5951	−14	4.510	0.000887	1.3019
Time to peak (s)	vii	0.7758 ± 0.1102	0.9050 ± 0.0740	17	−3.997	0.00210	1.1539
Time from peak (s)	viii	0.7225 ± 0.0976	0.6742 ± 0.0903	−7	2.259	0.0452	0.6521
d*F*/d*t* min (mN/s)	ix	−3.2661 ± 0.6324	−2.9205 ± 0.5919	−11	−2.696	0.0208	0.7783

Note: Values are animal-averaged mean ± SD. $N = 12$ mice (5 males and 7 females). Paired *t* tests. *d* = Cohen's *d* (paired, absolute value).

across cells. Sex-specific differences were assessed using two-way ANOVA (sex × treatment). No significant sex × treatment interactions were detected (interaction *P*-values reported in Table A1), justifying pooled analysis. Effect sizes (Cohen's *d*) were calculated for all paired comparisons. Statistical significance was set at $P < 0.05$. All analyses were performed using GraphPad Prism 10 (RRID:SCR_0 02798). Complete statistical details are provided in Tables 1 and A1–A7.

Results

Piezo1 activation selectively impairs force generation and contraction kinetics

To investigate how mechanotransduction regulates intestinal contractility, we performed wire myography on adult mouse small intestinal segments using two preparations (Fig. 1*A*): intact full-thickness segments containing all tissue layers (mucosa, submucosa, muscularis externa and serosa) and isolated muscularis externa preparations where the mucosa and submucosa were carefully removed while maintaining both smooth muscle layers and the myenteric plexus. Both preparations were mounted in organ baths containing oxygenated Krebs solution at 37°C under physiological preload conditions that support spontaneous phasic contractions. From these contractions we quantified steady-state control parameters (Fig. 1*B*) across several biomechanical domains. We recorded amplitude (peak force/contractile strength), integral force (cumulative mechanical work), frequency (contractions per minute) and period coefficient of variation (CV = SD/mean), a reflection of the temporal regularity of contraction spacing and duration.

Activation of Piezo1 with the selective agonist Yoda2 (25 μM; Qiao et al. (2025)) produced marked contractile dysfunction (Yoda2 concentration response, Table A2). Representative traces from male and female mice (Fig. 1*C*) show visibly reduced contraction amplitude following Yoda2 application, with contractions persisting at a similar frequency but diminished force. Responses appeared qualitatively similar between sexes, and exploratory analyses confirmed no significant sex × treatment interactions for any of the nine contractile parameters (interaction *P*-values in Table A1). Data from male and female mice were therefore pooled for all subsequent analyses. Because full-thickness intestinal preparations introduce variability from mucosal and submucosal cell populations that can influence contractile measurements independent of smooth muscle function, we used isolated muscularis externa preparations for all subsequent pharmacological experiments.

Paired *t* test analysis of the muscularis externa data (Fig. 1*D*; $N = 12$ mice, 5 males/7 females; full statistics in Table 1) revealed dysfunction across all three biomechanical domains. Peak contraction amplitude decreased 57% ($P = 1.37 \times 10^{-5}$; Fig. 1*Da*), and integral force decreased 56% ($P = 1.25 \times 10^{-6}$; Fig. 1*Db*), indicating substantially diminished capacity to generate the sustained mechanical energy required for normal intestinal motility (Sanders et al., 2012). In contrast to the large reductions in force, contraction frequency decreased by just 9% ($P = 0.0357$; Fig. 1*Dc*), and contraction duration increased by 10% ($P = 0.0100$; Fig. 1*De*), indicating that pacemaker-driven contraction events persist with only modest changes in their temporal profile. However the period CV% increased by 152% ($P = 0.0103$; Fig. 1*Dd*), revealing that although the pacemaker rhythm is maintained, the coupling between pacemaker signals and smooth muscle force output becomes less precise (Sanders, 2019).

The modest increase in contraction duration raises the question of whether Yoda2 slows the contractile cycle uniformly or selectively affects specific phases. Waveform kinetics revealed a striking asymmetry between the contraction and relaxation phases (Fig. 1*Df–i*). Peak contraction velocity (d*F*/d*t* max) decreased 14%

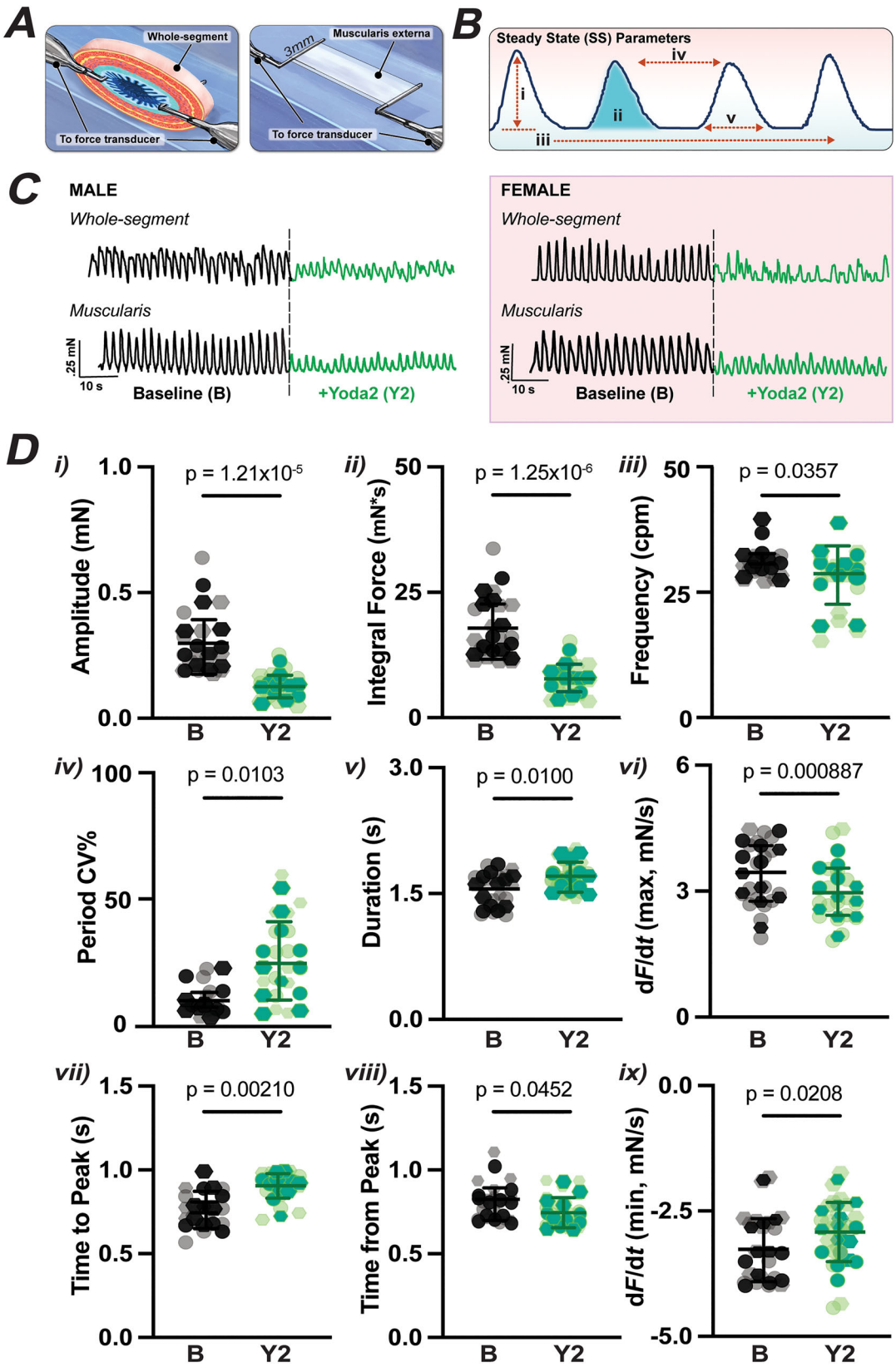

Figure 1. Piezo1 activation with Yoda2 selectively impairs force generation and slows the contraction phase in intestinal smooth muscle
A, schematic diagrams illustrating wire myography experimental preparations. Left: whole-segment preparation containing all tissue layers (mucosa, submucosa, muscularis externa and serosa) to preserve physiological tissue

architecture. Right: isolated muscularis externa preparation with mucosa and submucosa removed to eliminate non-muscle cell populations. *B*, primary contractile parameters depicted on schematic with the following definitions: (*a*) amplitude, peak force generated during each contraction cycle; (*b*) integral force, total area under all contractions representing cumulative mechanical work; (*c*) contraction frequency, number of contractions per minute; (*d*) period coefficient of variation (CV = SD/mean) to quantify cycle-to-cycle regularity of contraction spacing; and (*e*) duration, time from contraction onset to return to baseline. *C*, representative traces showing spontaneous phasic contractions at baseline (black) and after Yoda2 (25 μM, green) in whole-segment (top) and isolated muscularis (bottom) preparations from male (left) and female (right) mice. Scale bars: 0.25 mN, 10 s. *D*, contractile parameter analysis comparing baseline (black) *versus* Yoda2 (green). Males: circles; females: hexagons. Opaque symbols: per-animal averages; translucent: individual replicates. (*a–c*) Yoda2 reduced amplitude (57%), integral force (56%) and frequency (9%). (*d* and *e*) Temporal regularity decreased (period CV increased 152%; duration increased 10%). (*f–i*) Contraction velocity decreased (d*F*/d*t* max reduced 14%; time to peak increased 17%), whereas relaxation remained proportionally intact (d*F*/d*t* min reduced 11% *vs*. 57% amplitude decline). $n = 18$ preparations from $N = 12$ mice (5 males/7 females). Data: mean ± SD. Statistics: paired *t* tests on animal-averaged values. See Tables 1, A1 and A2 for complete statistics.

($P = 0.000887$; Fig. 1*Df*), and time to peak increased 17% ($P = 0.00210$; Fig. 1*Dg*), indicating that the force-generating upstroke is substantially slowed. In contrast the relaxation phase was preserved or relatively enhanced: time from peak decreased 7% ($P = 0.0452$; Fig. 1*Dh*), and although the absolute peak relaxation velocity (d*F*/d*t* min) decreased 11% in magnitude ($P = 0.0208$; Fig. 1*Di*), this small change accompanies a 57% reduction in amplitude, indicating that the tissue relaxes proportionally faster relative to the force it generates.

Together these data demonstrate that Piezo1 activation profoundly inhibits force generation and selectively slows the contraction phase relative to relaxation, raising the possibility that Yoda2 acts through intracellular Ca2+ handling pathways. Because Yoda2 is membrane permeant and therefore reaches Piezo1 in both compartments, we first asked which pool of Piezo1 carries this response, and then whether the response depends on SR Ca^{2+}.

Plasma membrane Piezo1 manipulation does not reproduce or prevent the Yoda2 contractile response

Because Yoda2 is membrane permeant and activates Piezo1 at both the plasma membrane and intracellular membranes, we used two membrane-impermeant tools to interrogate the plasma membrane pool selectively (Fig. 2). We first blocked plasma membrane Piezo1 with GsMTx4, a peptide that acts at the outer leaflet of the bilayer and does not cross the membrane (Bae et al., 2011; Gnanasambandam et al., 2017). GsMTx4 alone did not significantly change contractile parameters relative to baseline. Subsequent application of Yoda2 to GsMTx4-treated tissue still reduced contraction amplitude by 47% ($P = 0.0427$, baseline *vs*. Yoda2) and reduced the force integral relative to baseline ($P = 0.0181$), indicating that blocking the plasma membrane pool does not prevent the Yoda2 response.

We next asked whether selective activation of plasma membrane Piezo1 is sufficient to reproduce the response, using Jedi2, which gates Piezo1 through its extracellular blade domains and therefore engages the PM-facing pool (Wang et al., 2018). Jedi2 alone did not significantly alter amplitude, force or frequency ($N = 5$ mice per tool; all usable recordings from an animal were averaged to a single animal value before analysis). When Yoda2 was subsequently added to the same preparations, amplitude fell by 46% ($P = 0.0421$, baseline *vs*. Yoda2) and the force integral by 45% ($P = 0.0342$ *vs*. Jedi2), confirming that the tissue retained full capacity for Piezo1-mediated inhibition through the membrane-permeant agonist.

Blocking the plasma membrane pool therefore did not attenuate the Yoda2 response and activating that pool alone did not reproduce the contractile inhibition.

Piezo1-mediated contractile inhibition is attenuated by SR Ca^{2+} store disruption

We used two complementary approaches to disrupt SR Ca^{2+} signalling prior to Yoda2 application (Fig. 3). Thapsigargin (TG) irreversibly inhibits the sarcoplasmic/endoplasmic reticulum Ca^{2+}-ATPase (SERCA), passively depleting SR Ca^{2+} stores (Lytton et al., 1991), whereas ryanodine locks RyRs in a sub-conductance state, preventing physiological Ca^{2+} release (Rousseau et al., 1987). If Yoda2 acts through either of these SR Ca^{2+} pathways, pretreatment with either drug should reduce its contractile effects.

TG (10 μM), which depletes SR Ca^{2+} stores by irreversibly inhibiting SERCA, reduced contraction amplitude by 54% ($P = 0.00539$) and integral force by 51% ($P = 0.00182$; $N = 9$ mice, 4 males/5 females). Frequency was also reduced (23% decrease; $P = 0.0253$; Fig. 3*A* and *B*), suggesting that SR Ca^{2+} store content contributes to contraction initiation as well as force generation. The graded frequency effect in intact tissue contrasts with the isolated-cell recordings, in which Yoda2 evoked no significant current after TG pretreatment (Fig. 4*C* and *D*);

this is consistent with tissue-level contractile output arising from an electrically coupled network of smooth muscle and interstitial cells, such that the depletion of smooth muscle SR stores grades rather than eliminates the tissue response (Sanders et al., 2023). Subsequent Yoda2 application to TG-treated tissue produced additional reductions in amplitude (P = 0.00613), integral force (P = 0.0133) and frequency (P = 0.00451), demonstrating partial but incomplete occlusion of the Yoda2 response or contributions from non-SR sources such as plasma membrane Ca^{2+} entry.

Ryanodine at higher doses (100 μM) prevents physiological RyR-mediated Ca^{2+} release and produced a more uniform disruption, reducing amplitude by 61% (P = 0.000693), integral force by 61% ($P = 4.88 \times 10^{-5}$) and frequency by 50% (P = 0.00229; N = 10 mice, 5M/5F; Fig. 3*C* and *D*). The larger frequency reduction following ryanodine (50%) than following SR store depletion alone (23%) is consistent with RyR-mediated Ca^{2+} release contributing to the translation of pacemaker signals into co-ordinated smooth muscle contractions. After ryanodine pretreatment, subsequent Yoda2 application produced no further change in any metric (P = 1.000,

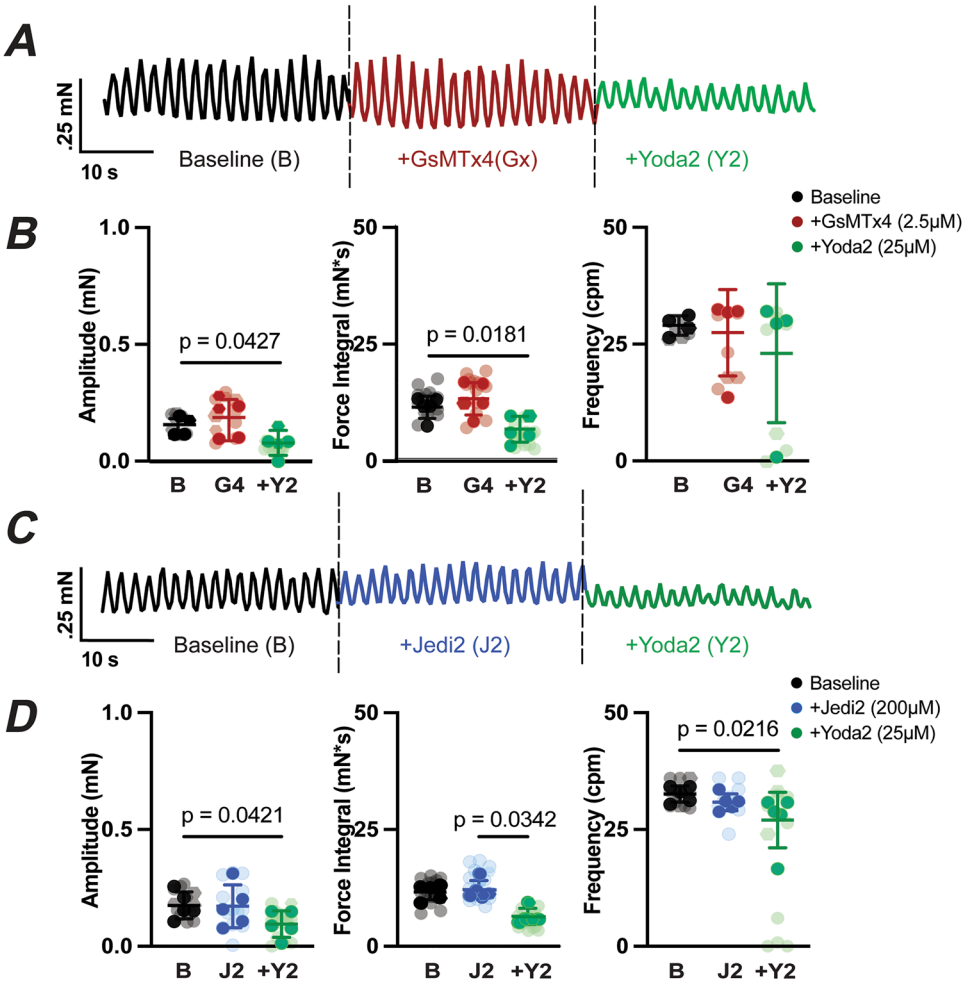

Figure 2. Membrane-impermeant tools do not reproduce or prevent the Yoda2 contractile response
A, representative traces showing baseline (black), GsMTx4 (2.5 μM, red) and Yoda2 (25 μM, green). Scale bars: 0.25 mN, 10 s. *B*, GsMTx4 did not significantly alter contractile parameters; subsequent Yoda2 reduced amplitude (P = 0.0427, baseline *vs*. Yoda2). Integral force was reduced relative to baseline (P = 0.0181, baseline *vs*. Yoda2), with no change in frequency. N = 5 mice per group; all usable recordings from an animal were averaged to a single animal value. *C*, representative traces showing baseline (black), Jedi2 (200 μM, blue) and Yoda2 (25 μM, green). Scale bars: 0.25 mN, 10 s. *D*, Jedi2 did not significantly alter contractile parameters; subsequent Yoda2 reduced amplitude (P = 0.0421, baseline *vs*. Yoda2) and integral force (P = 0.0342, Jedi2 *vs*. Yoda2), and frequency was reduced relative to baseline (P = 0.0216). N = 5 mice. Translucent symbols: individual preparations; opaque: animal averages. Data: mean ± SD. Statistics: repeated-measures one-way ANOVA with Geisser-Greenhouse correction and Holm–Šídák *post hoc*, or Friedman's test with Dunn's *post hoc* where normality was not met (see Table A3). Full statistics are provided in Table A3. B, baseline; Gx, GsMTx4; J2, Jedi2; Y2, Yoda2.

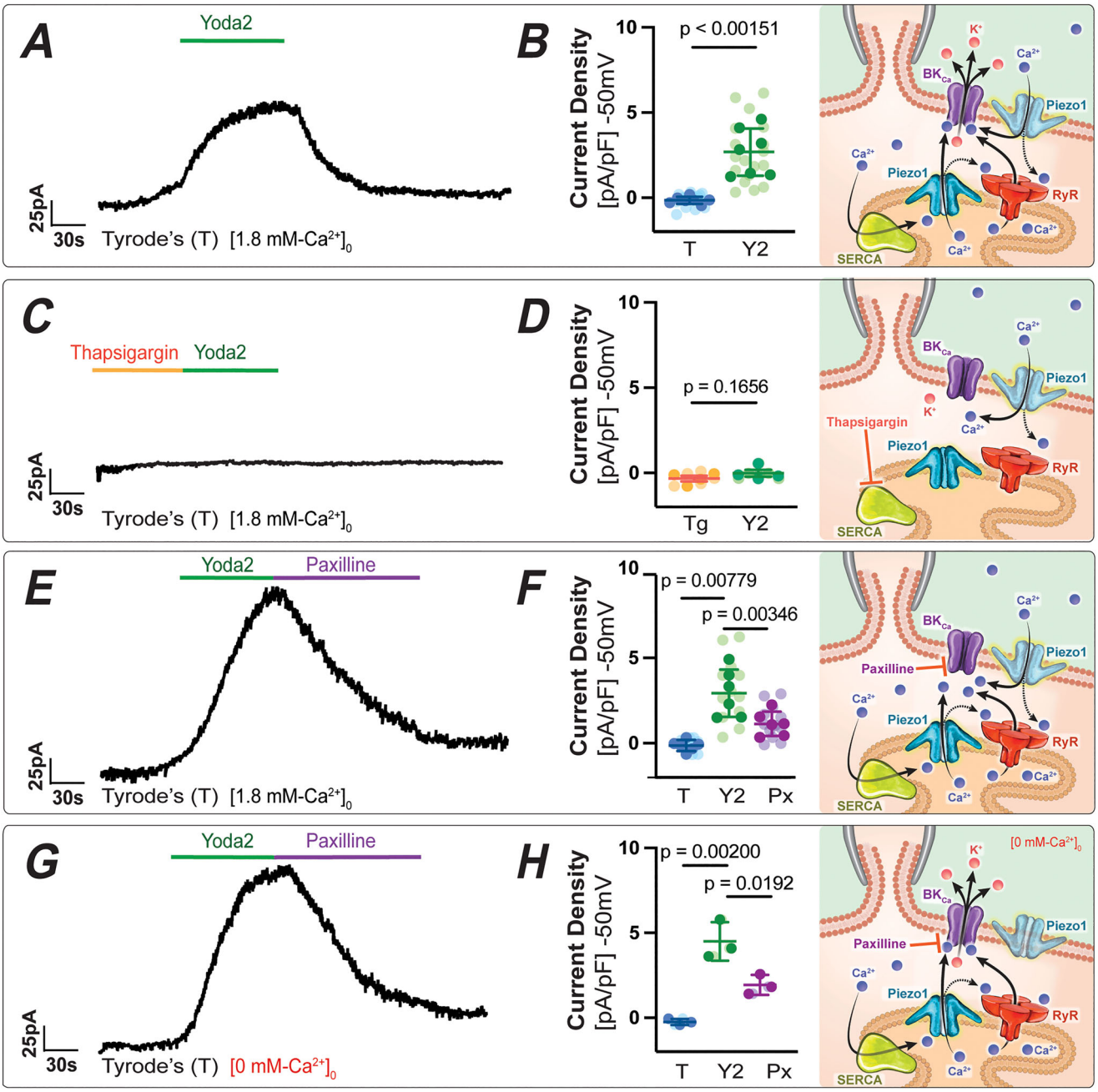

Figure 3. Sarcoplasmic reticulum (SR) Ca^{2+} store disruption attenuates Piezo1-mediated contractile inhibition (A,B) Thapsigargin
A, representative traces showing baseline (black), thapsigargin (10 μM) and Yoda2 (25 μM, green) effects. Scale bars: 0.25 mN, 60 s. *B*, thapsigargin reduced amplitude, integral force and frequency; subsequent Yoda2 produced further modest reductions. n = 11 segments from N = 9 mice (4 males and 5 females). (C,D) Ryanodine. *C*, representative traces showing baseline (black), ryanodine (100 μM, pink) and Yoda2 (25 μM, green). Scale bars: 0.25 mN, 60 s. *D*, ryanodine profoundly reduced all parameters; Yoda2 produced no additional effect. n = 14 segments from N = 10 mice (5 males and 5 females). Translucent symbols: individual preparations; opaque: animal averages. Data: mean ± SD. Statistics: repeated-measures one-way ANOVA with Geisser-Greenhouse correction and Holm–Šídák *post hoc*, or Friedman's test with Dunn's *post hoc* where normality was not met. $P < 0.05$ values considered significant.

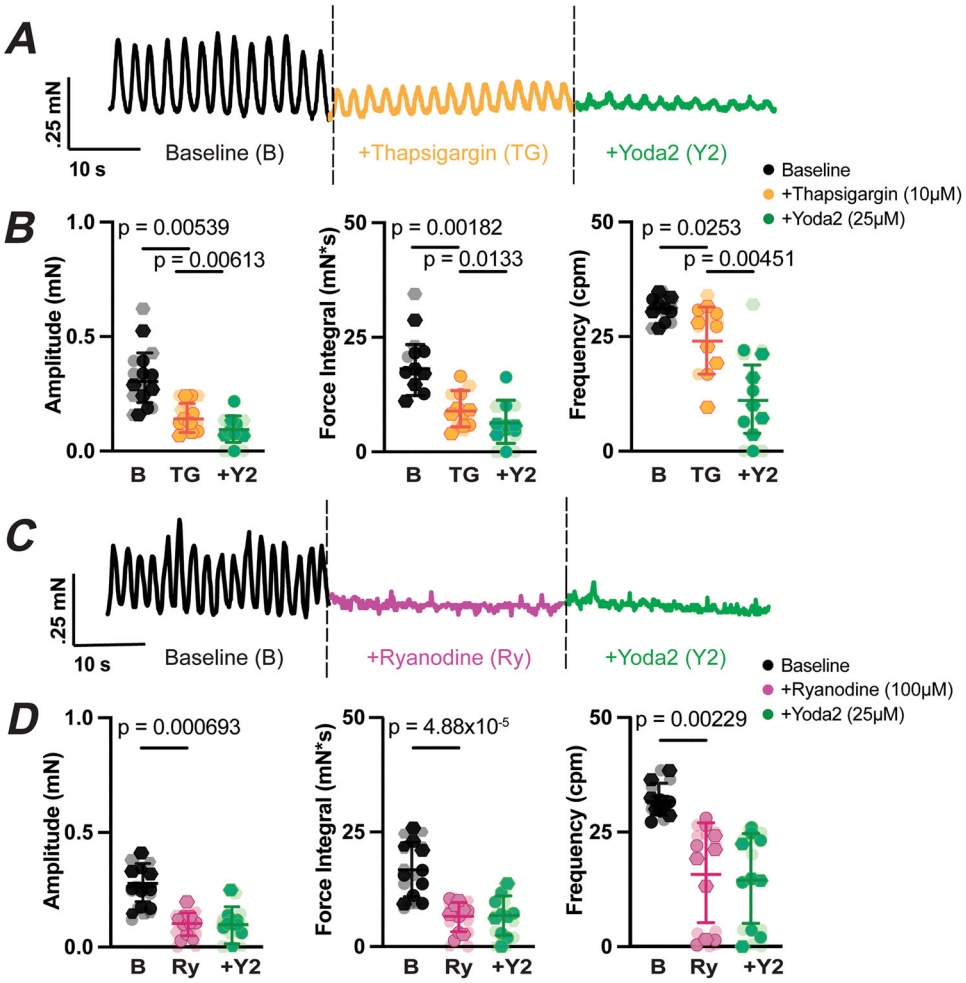

Figure 4. Piezo1 activation produces BK channel-mediated outward currents that require sarcoplasmic reticulum (SR) Ca^{2+} and persist in 0 mM extracellular Ca^{2+}
(A,B) Yoda2 evokes outward currents in intestinal smooth muscle cells (ISMCs). *A*, representative whole-cell patch-clamp current recording from a freshly dissociated ISMC voltage-clamped at −50 mV in Tyrode's III solution at baseline, in response to Yoda2 (10 μM, green bar) and after washout. *B*, current density (pA/pF) at baseline (T) and peak Yoda2-evoked currents (Y2). Paired *t* test; *N* = 7 mice, *n* = 18 cells. The schematic depicts the proposed signalling pathway: Piezo1-mediated Ca^{2+} entry and/or intracellular store release activate ryanodine receptors (RyR) and/or directly activate BK_{Ca} channels. (C,D) SR Ca^{2+} store depletion attenuates the Yoda2 response. *C*, representative recording from a cell preincubated with thapsigargin (TG) and voltage-clamped at −50 mV at baseline, in response to Yoda2 and washout. *D*, current density at baseline with TG during Yoda2. Paired *t* test; *N* = 5 mice, *n* = 7 cells. Schematic illustrates that SERCA inhibition with TG results in depletion of intracellular Ca^{2+} necessary for Yoda-evoked Piezo1 activation of outward current. (E,F), BK channel blockade reduces Yoda2-evoked currents in 1.8 mM Ca^{2+}. *E*, representative currents recorded at baseline, with Yoda2 (10 μM, green bar) and subsequent addition of paxilline (10 μM, purple bar). *F*, current density at baseline (T), with Yoda2 (Y2) and with paxilline (Px). Repeated-measures (RM) one-way ANOVA; *N* = 6 mice, *n* = 10 cells. Schematic illustrating that paxilline inhibits downstream BK_{Ca} channels, whereas the Piezo1-RyR Ca^{2+} release pathway remains intact, reducing outward current density. (G,H) Yoda2-evoked, paxilline-sensitive currents persist without extracellular Ca^{2+}. *G*, representative recording at baseline, after acute removal of extracellular Ca^{2+}, during Yoda2 (green bar), after paxilline (purple bar) and after washout. *H*, current density at baseline in 0 mM Ca^{2+} (T), peak Yoda2 (Y2) and after paxilline (Px). *N* = 3 mice. Schematic illustrates that $[Ca^{2+}]_i$ store released through RyR sustains BK_{Ca} activation in absence of extracellular Ca^{2+} entry, and paxilline reduces the outward current. Individual cells are shown as translucent dots with opaque dots for per-animal averages; data shown as mean ± SD. *P*-values are as indicated above, with $P < 0.05$ considered significant.

0.803 and 0.542 for amplitude, integral force and frequency, respectively; Table A4). Whether a floor effect from ryanodine depletion of contractile reserve prevents further Yoda2 inhibition cannot be fully excluded.

These data are consistent with Yoda2 and ryanodine acting through overlapping pathways in which Piezo1 triggers additional SR Ca^{2+} release via RyR, thereby 'amplifying' the $[Ca^{2+}]_i$ to collectively activate BK_{Ca} (Dopico et al., 2018; Santana et al., 1996). However the variable effects of ryanodine probably stem from its complex, concentration-dependent actions and other explanations, such as ryanodine interfering with pacemaker mechanisms independently of Piezo1, are also possible (Collier et al., 2000).

Taken together with the predominantly intracellular localization of Piezo1 and the SR store dependence of the Yoda2-evoked current, both established below, these results provide convergent pharmacological evidence that the contractile inhibition originates largely from intracellular Piezo1, supporting the hypothesis that Piezo1 mobilizes SR Ca^{2+} to activate hyperpolarizing conductances that inhibit contractility. However wire myography cannot resolve the underlying cellular mechanism due to the complex nature of intact tissue and the presence of Piezo1 in several layers and cell types within the intestinal muscularis. It remains unresolved whether Piezo1 directly triggers SR Ca^{2+} release, activates downstream Ca^{2+}-sensitive conductances or both. To address this we performed whole-cell patch-clamp recordings on isolated SMCs to determine whether Piezo1 activation produces identifiable ionic currents that would explain these contractile effects.

Piezo1 activation produces paxilline-sensitive outward currents in isolated small intestinal SMCs

To investigate the cellular mechanisms underlying Piezo1-mediated contractile inhibition we performed whole-cell patch-clamp recordings on freshly isolated SMCs to determine whether Piezo1 activation produces outward (hyperpolarizing) currents that would lead to relaxation in GI smooth muscle.

At −50 mV PM Piezo1 activation would be expected to produce inward (negative) current from Ca^{2+} and Na^{+} influx (Coste et al., 2010; Gnanasambandam et al., 2015), which would depolarize the membrane and potentially trigger voltage-gated Ca^{2+} channels to enhance contraction. Instead application of the Piezo1 agonist Yoda2 (10 μM) produced marked outward (positive) currents that developed over 30–60 s and returned to baseline upon washout (Fig. 4*A*). Addition of Yoda2 significantly increased current density from −0.30 ± 0.36 pA/pF at baseline to 2.49 ± 1.81 pA/pF during Yoda2 application ($P = 0.00151$; $n = 18$ cells from $N = 7$ mice; Fig. 4*B*). The outward direction indicates K^{+} efflux, which would hyperpolarize the membrane and reduce voltage-gated Ca^{2+} channel activity, consistent with the contractile inhibition observed in tissue recordings.

To test whether the Yoda2-evoked outward current requires SR Ca^{2+} stores cells were preincubated with TG (1 μM, 20 min) to impair SR Ca^{2+} uptake and deplete releasable SR Ca^{2+} before recording. After TG pretreatment cells were perfused continuously with the TG-containing solution to maintain store depletion throughout the recording (Fig. 4*C*). Under these conditions Yoda2 application did not significantly alter current density ($P = 0.166$; $n = 7$ cells from $N = 5$ mice; Fig. 4*D*), indicating that functional SR Ca^{2+} stores are required for Piezo1-mediated outward currents.

The outward current kinetics and $[Ca^{2+}]_i$ dependence are consistent with BK channel activation, which is driven by local Ca^{2+} release events (Ca^{2+} sparks) in smooth muscle (Gollasch et al., 1998; Nelson et al., 1995). We therefore tested this by applying paxilline (10 μM), a selective BK channel blocker that acts by stabilizing the closed conformation (Zhou & Lingle, 2014), during the Yoda2 response, which significantly reduced the Yoda2-evoked current from 2.83 ± 1.39 to 1.04 ± 0.71 pA/pF ($P = 0.00346$; $n = 10$ cells from $N = 6$ mice; Fig. 4*E* and *F*).

To determine whether the Yoda2-induced current requires Ca^{2+} influx from the extracellular space we switched to Ca^{2+}-free Tyrode's III after an initial 30 s baseline was established. In 0 $[Ca^{2+}]_o$ external solution Yoda2 still produced robust outward currents (4.82 ± 1.18 pA/pF *vs.* −0.11 ± 0.19 pA/pF at baseline; $P = 0.00200$; $N = 3$ mice; Fig. 4*G* and *H*). Subsequent application of paxilline (10 μM) reduced current density to 2.15 ± 0.61 pA/pF ($P = 0.0192$), representing 54% inhibition of the Yoda2-induced increase. The persistence of Yoda2-evoked, paxilline-sensitive outward currents under Ca^{2+}-free conditions suggests that extracellular Ca^{2+} entry is not the main trigger. Instead it points to intracellular Ca^{2+} release as the source for activating BK channels. However the possibility that residual extracellular Ca^{2+} or Ca^{2+} that entered prior to the solution change cannot be entirely ruled out.

Together these electrophysiological findings reveal that Piezo1 activation in small ISMCs produces outward K^{+} currents that would be expected to hyperpolarize the membrane and inhibit contractility. The BK channel-mediated outward currents suggest the involvement of SR Ca^{2+} signalling, as BK channel activation in smooth muscle typically occurs through Ca^{2+} spark-mediated local Ca^{2+} elevations. To determine whether Piezo1, RyR and BK channels are positioned close enough to support this local signalling mechanism we

next examined their spatial relationships using immunofluorescence and PLAs.

Piezo1 predominantly localizes to intracellular membranes in intestinal SMCs

To determine whether the functional coupling between Piezo1, SR Ca^{2+} release and BK channel activation observed (Figs 1–4) reflects specific subcellular organization we examined the spatial distribution of Piezo1, RyR and BK_{Ca} in freshly isolated ISMCs from Piezo1-tdTomato reporter mice. Piezo1 localization was detected using anti-RFP antibodies against the TdTomato reporter, which provided more reliable targeting than direct Piezo1 antibodies, given challenges with Piezo1 immunolocalization (Alper, 2017).

Immunocytochemical labelling (Fig. 5*A*) revealed that Piezo1 clusters (anti-RFP, cyan) were predominantly distributed within intracellular compartments rather than at the plasma membrane, following a pattern similar to that of RyR (magenta; Fig. 5*A*). Quantitative analysis performed using surface-based classification algorithms (Imaris, ±2 pixel threshold relative to membrane surface) in $n = 48$ cells from $N = 10$ mice (5 males/5 females) showed that 86.15 ± 7.28% of Piezo1 clusters were intracellular (cyan) compared to 13.85 ± 7.28% at the plasma membrane (blue; paired t test on per-animal means, $t(9) = 21.98$, $P = 3.94 \times 10^{-9}$; Fig. 5*B* and *E*). Similarly RyR immunoreactivity was detected predominantly in intracellular compartments (magenta) rather than near the plasma membrane (red; $t(9) = 17.64$, $P = 2.74 \times 10^{-8}$; Fig. 5*C* and *F*). This predominant intracellular distribution of both Piezo1 and RyR is consistent with SR localization and with the functional requirement for SR Ca^{2+} stores, as demonstrated by TG sensitivity (Figs 3, 4*C* and *D*). No significant sex differences were detected for any parameter (comparison of the plasma membrane value between sexes, $N = 5$ *vs.* 5; $P = 0.818$, 0.743, 0.548 and 0.901 for panels 5*E*–5*H*, respectively; Table A6A). Because the plasma membrane and intracellular percentages are complementary fractions of the same cluster population, the comparison in panels 5*E* and 5*F* tests whether the distribution departs from an even split rather than comparing two independent quantities.

To determine whether Piezo1 and RyR occupy similar subcellular domains we quantified clusters exhibiting spatial overlap (centre-to-centre distance < 240 nm) separately for membrane and intracellular compartments (Fig. 5*D*). Colocalized Piezo1-RyR clusters were approximately fivefold more abundant in the intracellular compartment compared to the plasma membrane (paired t test on per-animal means, $t(9) = 13.50$, $P = 2.80 \times 10^{-7}$; Fig. 5*G*). The same enrichment held when colocalization was expressed as a percentage of Piezo1 clusters: approximately 10% of intracellular clusters colocalized with RyR *versus* approximately 2% at the PM (paired t test on per-animal means, $t(9) = 14.47$, $P = 1.54 \times 10^{-7}$; Fig. 5*H*). These data indicate that Piezo1 and RyR are not merely co-distributed within the same cellular compartment but preferentially co-assemble within intracellular domains.

Although confocal microscopy (resolution limit ∼200 nm) can resolve colocalization at the subcellular level, it cannot determine whether proteins are positioned within the <100 nm range typical of functional Ca^{2+} coupling domains. To address this limitation we employed PLA, which generates fluorescent puncta only when two target proteins are within <40 nm of each other (Fig. 6*A* and *B*). For these experiments PLA image pairs were analysed using per-animal means across independent biological cohorts ($N = 11$ mice for the RyR-Piezo1 pair; $N = 12$ mice for the BK_{Ca}-Piezo1 pair). RyR-Piezo1 PLA signal was significantly elevated compared to single-antibody controls (one-way ANOVA on per-animal means with Holm–Šídák *post hoc*; $P = 0.0288$ *vs.* RyR-only and $P = 0.0288$ *vs.* Piezo1-only; Fig. 6*C*), confirming nanoscale proximity between these two channels. BK_{Ca}-Piezo1 PLA signal was similarly elevated compared to controls ($P = 0.0280$ *vs.* BK_{Ca}-only and $P = 0.0280$ *vs.* Piezo1-only; Fig. 6*D*). These data also support the previous finding that the majority of Piezo1 channels in jejunal SMCs are expressed in intracellular compartments, as indicated by the greater number of PLA puncta detected far from the nearest plasma membrane site (Fig. 6*F–J*). Notably BK_{Ca}-Piezo1 proximity was approximately twofold more abundant than RyR-Piezo1 proximity ($P = 0.00718$; Fig. 6*E*), suggesting a stoichiometry consistent with the established model of Ca^{2+} spark-STOC coupling, in which multiple BK channels must be activated by a single Ca^{2+} release event to produce a physiologically meaningful hyperpolarization (Brenner et al., 2000).

Collectively these data indicate that RyR and BK_{Ca} each reside within <40 nm of Piezo1 at intracellular sites, providing the nanoscale spatial framework required for the SR Ca^{2+} store-dependent, BK-mediated outward currents recorded in Fig. 4.

Discussion

This study identifies a functional intracellular mechanotransduction axis in small intestinal smooth muscle, defined by a specialized signalling complex on the SR, comprising intracellular Piezo1 (intra-Piezo1) and RyR, in complex with PM BK_{Ca} channels (Fig. 7). Three convergent lines of evidence support this conclusion. First, Piezo1 activation with Yoda2 reduced contractile force and slowed contraction kinetics at the tissue level,

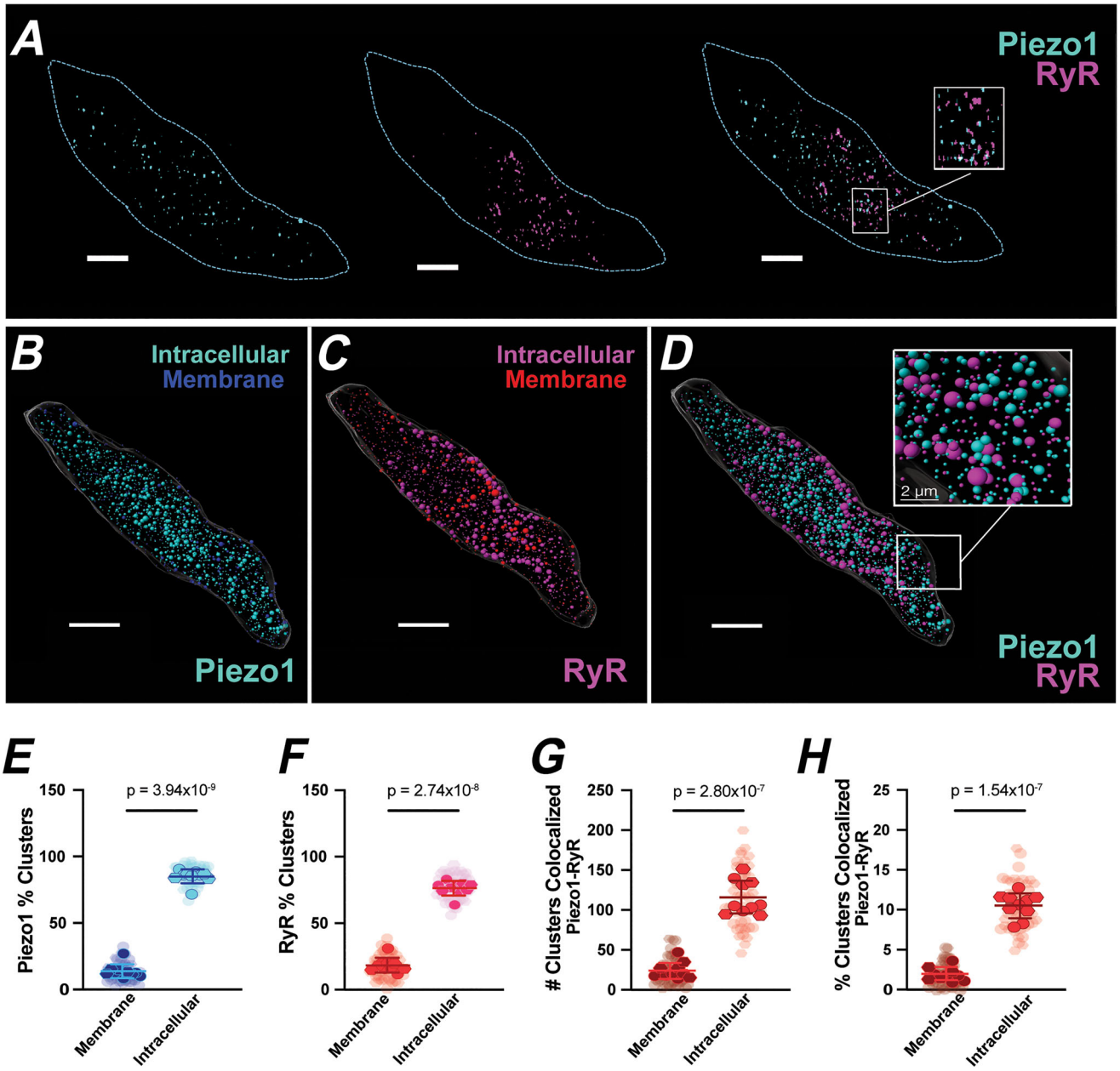

Figure 5. Piezo1 localizes predominantly intracellularly with nanoscale proximity to ryanodine receptor (RyR) and BK channels
(A–D) Confocal microscopy of jejunal circular smooth muscle from Piezo1-tdTomato mice. *A*, left to right: Piezo1-tdTomato (cyan), RyR (magenta) and merge, with insets showing colocalization. Scale bars: 10 µm; inset 2 µm. (B,C) Imaris three-dimensional (3-D) surface classification separating membrane-localized (*B*, Piezo1 blue, RyR red) from intracellular (*C*, Piezo1 cyan, RyR magenta) signal. *D*, merged view showing extensive intracellular colocalization between Piezo1 (cyan) and RyR (magenta). (E–H) Quantification of Piezo1/RyR cluster distribution and association for $n = 48$ cells from $N = 10$ animals: percentage of Piezo1 (*E*) and RyR (*F*) clusters localized at the plasma membrane (± 2 voxels) or intracellular compartments; the number (*G*) and percentage (*H*) of all Piezo1 clusters colocalized with RyR, either at the plasma membrane or intracellularly. Statistics: *P*-values are as indicated above, with $P < 0.05$ marked as significant. Translucent symbols: individual cells; opaque: animal averages. Data: mean ± SD. Data analysed from $n = 48$ cells from $N = 10$ mice (5 males and 5 females). Compartment comparisons were made using paired *t* test on per-animal means ($N = 10$, $dF = 9$). Sex was tested by comparing the plasma membrane value between sexes ($N = 5$ *vs*. 5); no sex effect reached significance for any parameter (Table A6A). Mean ± SD are computed across cells.

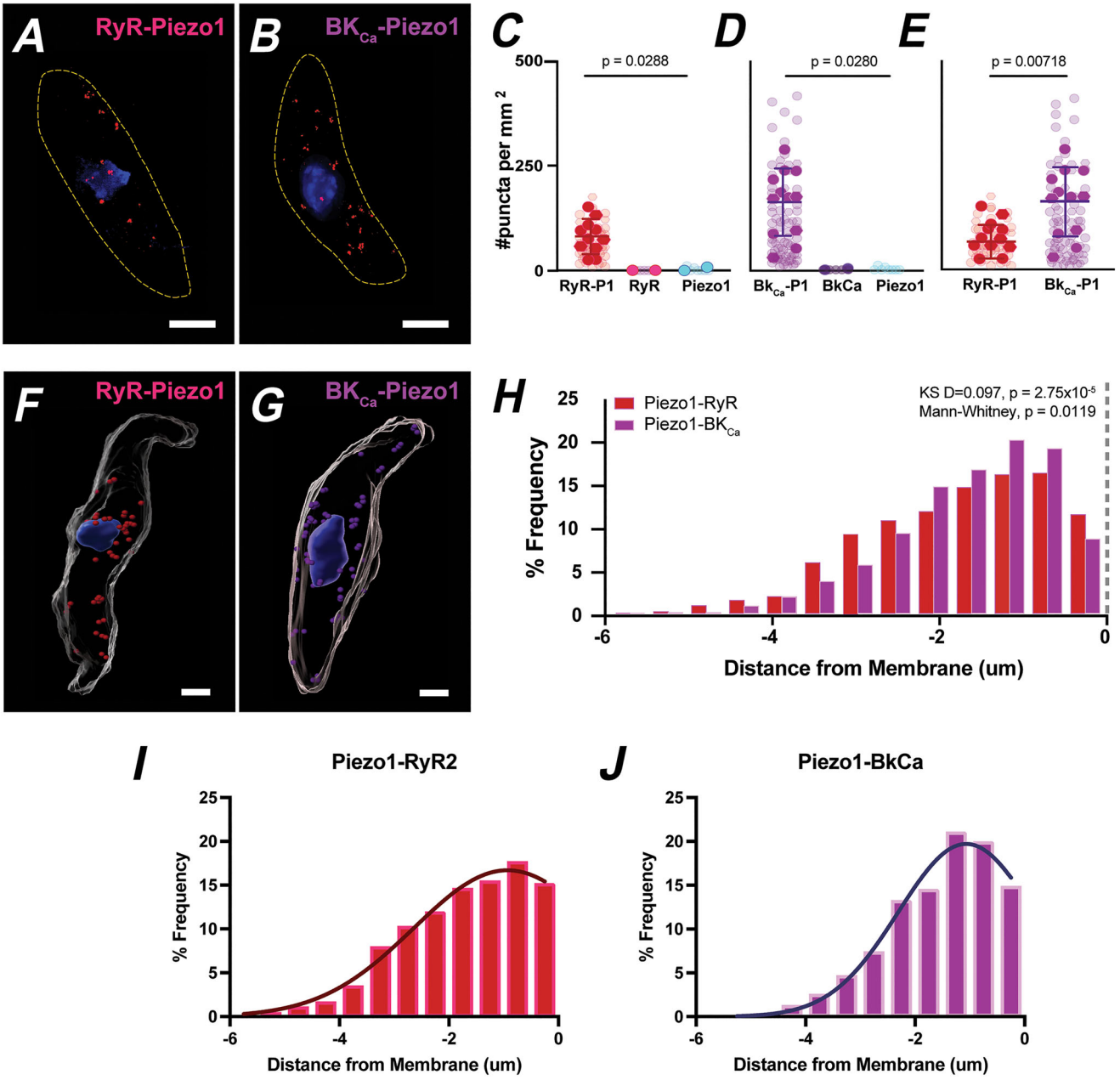

Figure 6. Proximity ligation assay (PLA) confirms nanoscale association of intracellular Piezo1 with ryanodine receptor (RyR) and BK_{Ca}
(A,B) Representative maximum-intensity projections of PLA puncta (red) with nuclei (DAPI, blue): (*A*) RyR-Piezo1 and (*B*) BK_{Ca}-Piezo1. *C*, RyR-Piezo1 puncta density (puncta/mm^2) *versus* single-antibody controls (N = 11 mice; P = 0.0288; P = 0.0288). *D*, BK_{Ca}-Piezo1 puncta density *versus* single-antibody controls (N = 12 mice; P = 0.0280; P = 0.0280). *E*, direct comparison of RyR-Piezo1 *versus* BKCa-Piezo1 (P = 0.00718). (F,G) Representative three-dimensional (3-D) surface reconstructions: (*F*) RyR-Piezo1, (*G*) BK_{Ca}-Piezo1. *H*, frequency distribution of puncta distance from the plasma membrane, Piezo1-RyR *versus* Piezo1-BK_{Ca} (KS D = 0.097, $P = 2.75 \times 10^{-5}$; Mann–Whitney P = 0.0119). (I,J) Distance-from-membrane distributions with fitted curves: (*I*) Piezo1-RyR2 and (*J*) Piezo1-BK_{Ca}. Mean puncta density: RyR-Piezo1: 81.49 ± 40.44; BK_{Ca}-Piezo1: 161.82 ± 80.35 puncta/mm^2. Translucent symbols: individual cells; opaque: animal averages. Data are presented as mean ± SD, where metrics reflect per-animal values, and SD denotes interanimal variability. Statistics: ordinary one-way ANOVA on per-animal means with Holm–Šídák *post hoc* (*C*, *D*); Welch's unpaired *t* test (*E*).

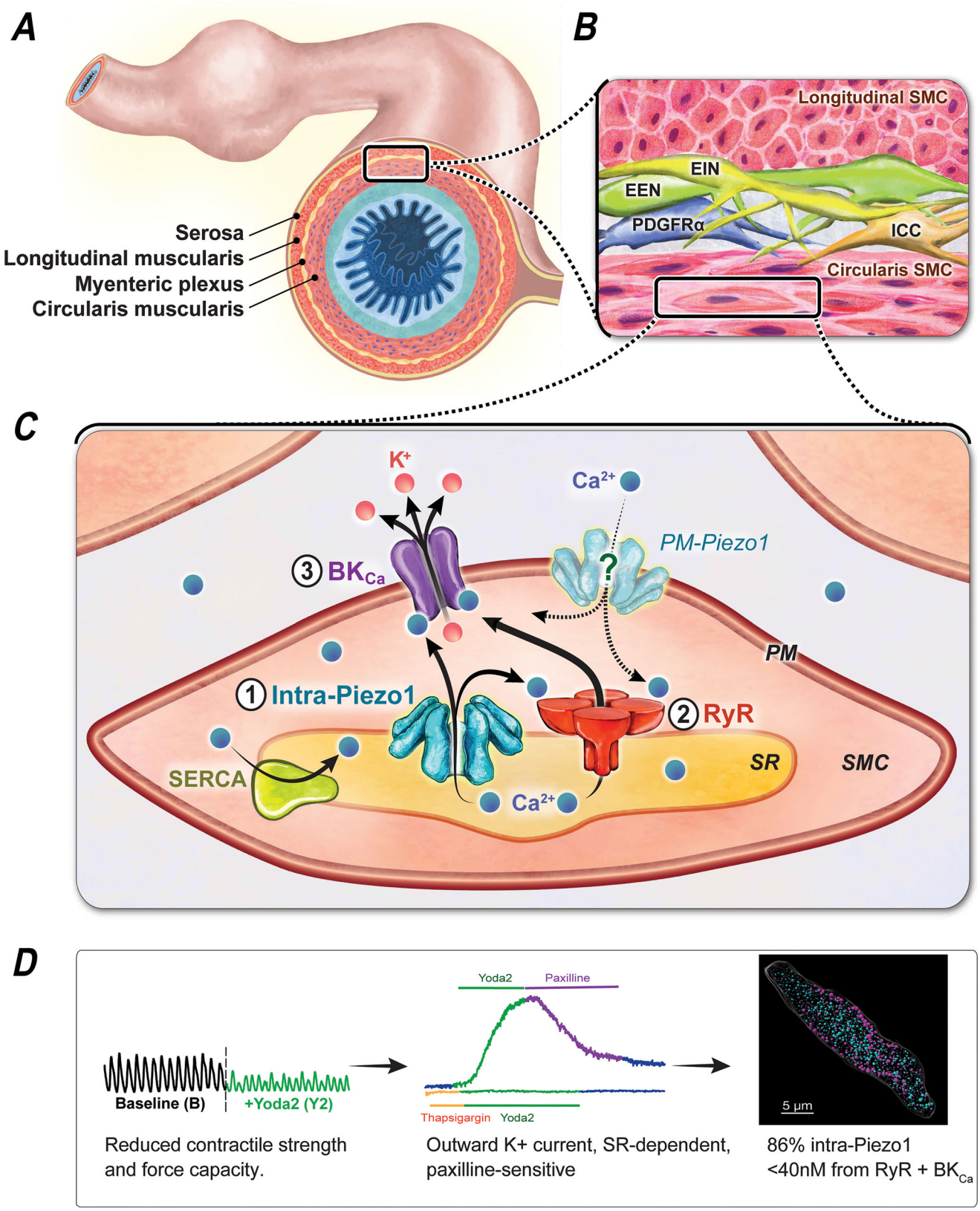

Figure 7. Proposed multiscale model of mechanotransduction in gastrointestinal (GI) smooth muscle, from tissue to nanoscale microdomains
A, tissue-level mechanosensation. The intestinal wall undergoes continuous mechanical strain generated by luminal distension, fluid shear stress, and active peristalsis. *B*, cellular integration within the muscularis. Mechanical stimuli

are integrated across the electrically coupled network of smooth muscle cells (SMCs), interstitial cells of Cajal (ICC) and PDGFRα^+cells, termed the "SIP" syncytium, with enteric neuronal input (excitatory, EEN; inhibitory, EIN) to coordinate tissue-level motor patterns. *C*, subcellular working model of the mechanosensitive 'molecular brake'. Within an individual SMC, a specialized 'sensor–amplifier–effector' complex is localized to the nanoscale gap of the sarcoplasmic reticulum-plasma membrane (SR–PM) junctional nanodomain. (1) SENSOR: intra-Piezo1 activation triggers an initial Ca^{2+}release from intracellular stores in SR. (2) AMPLIFIER: ryanodine receptors (RyRs) are subsequently activated via calcium-induced calcium release (CICR), amplifying the junctional Ca^{2+} transient. (3) BK_{Ca} triggered by locally amplified Ca^{2+}, resulting in K^+ efflux; SERCA maintains SR Ca^{2+} content to sustain the signalling loop. In GI SMCs this hyperpolarization leads to dampening of cellular excitability to prevent hyper-contractility and ensure co-ordinated relaxation via reverse signalling back to the tissue level ($C \rightarrow B \rightarrow A$). *D*, summary of key findings presented.

consistent with the engagement of a relaxation pathway rather than excitatory surface-channel activity. Second, Piezo1 activation evoked outward currents that required intact SR Ca^{2+} stores, persisted without extracellular Ca^{2+} and were subtantially reduce by the BK_{Ca} channel inhibitor paxilline, placing the signal origin at the SR. Third, high-resolution imaging and PLAs revealed that ∼86% of Piezo1 clusters reside intracellularly, colocalize with RyR and are positioned within <40 nm of both RyR and BK_{Ca} channels.

These findings describe a physiological axis in smooth muscle and provide functional evidence that organelle mechanosensation proceeds through intracellular Piezo1 (intra-Piezo1). The canonical view posits that Piezo1-mediated mechanotransduction is initiated exclusively at the PM via cation influx (Coste et al., 2010; Gudipaty et al., 2017). Our work identifies an alternative intracellular pathway for SMC mechanosensitivity, mediated by intra-Piezo1. In small intestinal smooth muscle, activating this pathway engages SR Ca^{2+} release and BKca-mediated hyperpolarization that reduced contractile force, that we identify as a 'sensor–amplifier–effector' complex: intra-Piezo1 (sensor), RyRs (amplifier) and BK_{Ca} channels (effector). Activation of intra-Piezo1 would result in Ca^{2+} release from the SR into the cytosol, and the localized Ca^{2+} release would then trigger RyR to activate Ca^{2+}-induced Ca^{2+} release (CICR) at other nearby RyRs. The resulting amplified Ca^{2+} pool would then activate BK_{Ca} channels, leading to membrane hyperpolarization and muscle relaxation (Nelson et al., 1995; Ríos, 2018). An equivalent Piezo1-to-BK arrangement operates in other native tissues: in the distal nephron PIEZO1 mediates flow-induced Ca^{2+} entry and is required for BK-dependent K^+ secretion (Carrisoza-Gaytan et al., 2024); in pulmonary arterial endothelium BK channels colocalize with Piezo1, and their deletion blunts Piezo1-mediated Ca^{2+} influx (Guntur et al., 2025); and in sensory neurons Piezo1-evoked Ca^{2+} influx activates $K_{Ca}1.1$ in a manner reversed by iberiotoxin (Liu et al., 2026). Functional complexes between Piezo1- and Ca^{2+}-activated channels have now been described across several cell types and are increasingly regarded as a general feature of Piezo1 signalling (Vasileva et al., 2025).

The proposed intracellular axis functions as a molecular brake, coupling organellar mechanosensing via intra-Piezo1 to BK_{Ca}-mediated hyperpolarization to dampen excitability and promote relaxation (Fig. 7). This resolves the paradox of why knocking out Piezo1 channels in ISMCs leads not only to contractile deficits but also to complex ion-channel remodelling that creates a hyperexcitable environment (Bautista et al., 2025). Such profound, indirect consequences establish that organelles are active participants in detecting and regulating stress from the inside out.

Intracellular Piezo1: evidence for a subcellular signalling hub

The predominantly intracellular localization of Piezo1 in intestinal smooth muscle is not an isolated finding. Growing evidence demonstrates that Piezo1 functions within intracellular compartments across diverse cell types, suggesting that this dual localization reflects a conserved property of the channel (Bautista et al., 2026).

The most direct smooth muscle precedent comes from pulmonary arterial smooth muscle cells (PASMCs), where Liao et al. (2021) demonstrated Piezo1 colocalization with ER/SR, mitochondrial and nuclear envelope markers, with Yoda1-evoked Ca^{2+} transients persisting in Ca^{2+}-free medium and abolished by Piezo1 small interfering RNA (siRNA) knockdown. In epithelial cells McHugh et al. (2010) used subcellular fractionation and ER marker co-enrichment to localize Fam38A/Piezo1 to the ER in HeLa and CHO cells, where it recruits R-Ras, increases Ca^{2+} release from cytoplasmic stores to activate calpain and triggers $\beta 1$ integrin activation through talin cleavage, an inside-out signalling pathway with consequences for cell adhesion and migration (McHugh et al., 2010; McHugh et al., 2012). This diversity of locations and functional outputs, ranging from definitive organellar residence to functional coupling, argues against a trafficking artifact, as biosynthetic intermediates would not produce such organelle-appropriate signalling across cell types.

Piezo1's biophysical properties rationalize how the channel operates at intracellular membranes. Its large

structural footprint and curvature sensitivity favour low-curvature membranes such as the ER/SR, and its capacity for conformational signalling, mechanical rearrangement of propeller domains independent of ion flux, enables mechanotransduction at organellar membranes with ionic compositions distinct from the extracellular space (Guo & MacKinnon, 2017; Lewis et al., 2024). Critically the ER/SR membrane is not mechanically isolated: it experiences direct tension as part of a coupled membrane continuum, with PM curvature regulating ER contact formation (Townson & Progida, 2025; Yang et al., 2024). In endothelial cells Piezo1 promotes ER Ca^{2+} transport in response to shear stress through an IP_3R2-dependent circuit (Santana Nunez et al., 2023), and in the *Drosophila* heart Piezo buffers mechanical stress through intracellular Ca^{2+} modulation rather than surface currents (Zechini et al., 2022). Together these findings establish that mechanical force can reach and gate intracellular Piezo1 across organ systems and species (Bautista et al., 2026). The resting curvature and force threshold of PIEZO1 are set, in part, by a PIP2-co-ordinated interaction between adjacent blades, so the lipid composition of the host membrane, rather than the channel alone, determines its mechanical set point (Smith et al., 2025). Direct tension measurement further shows that the ER both relays and buffers the membrane tension reaching internal compartments (Shen et al., 2026).

A unifying principle emerges: Piezo1 operates as a mechanosensory hub, with its subcellular address and nanodomain partners dictating the direction and magnitude of its output. This model, in which the same channel produces hyperpolarization from the SR and depolarization from the plasma membrane, resolves the long-standing paradox of how a single ion channel can promote both proliferation and apoptosis, contraction and relaxation (Gudipaty et al., 2017).

The pharmacological dissection supports a dual-function arrangement. Selective activation of the plasma membrane pool with Jedi2 did not reproduce the contractile suppression produced by the membrane-permeant agonist Yoda2, and inhibition of surface mechanosensitive channels with GsMTx4 did not prevent it, together indicating that the inhibitory response is driven predominantly by the intracellular channel population. Jedi2 alone did not significantly alter contractile activity, although the direction of the observed change suggests a potential model in which the plasma membrane pool of Piezo1 contributes excitatory influence, whereas the intracellular pool drives inhibition. The study was not powered to detect an effect of this size, and the small number of preparations leaves us unable to separate genuine excitation from noise, so we treat this observation as hypothesis-generating rather than conclusive. We therefore interpret the surface-pool manipulations as supportive of a dual contribution rather than definitive.

The nanoscale architecture of the organellar mechanosensory niche

The sensor–amplifier–effector complex we describe is built upon a well-characterized foundation of nanoscale Ca^{2+} signalling at PM–SR junctions, a fundamental organizing principle of smooth muscle physiology. Within the ∼20 nm gap of peripheral junctions localized Ca^{2+} sparks from RyR in the SR activate clustered BK_{Ca} channels on the overlying PM, producing spontaneous transient outward currents (STOCs) that oppose voltage-gated Ca^{2+} entry and constrain myogenic tone, establishing the paradigm of spatially restricted Ca^{2+} coupling in vascular smooth muscle (Jaggar et al., 2000; Nelson et al., 1995; Santana et al., 1996). This system requires nanometre-scale co-assembly of RyR and BK_{Ca} channels at junctional sites organized by scaffolding proteins such as junctophilin-2 (Chen et al., 2026; Kotlikoff, 2003; Pritchard et al., 2019; Santana et al., 1996).

In the GI tract BK_{Ca} channels function as essential brakes on excitability (Meredith et al., 2006; Ren et al., 2016; Wang et al., 2010), yet their precise contributions and activation mechanisms vary across intestinal segments. BK_{Ca} channel function is best characterized in the colon, where the inhibitory architecture differs fundamentally from the classical RyR-BK_{Ca} spark-STOC paradigm. In colonic smooth muscle spontaneous Ca^{2+} transients are IP_3R-mediated Ca^{2+} puffs that couple to spontaneous transient outward currents through both BK_{Ca} and small-conductance SK channels (Bayguinov et al., 2000; Bayguinov et al., 2001; Koh et al., 1998). However in the small intestine STOCs are driven instead by RyR-dependent Ca^{2+} sparks that couple directly to BK_{Ca} channels (Benham et al., 1986; Bolton & Lim, 1989; Nelson et al., 1995), with localized Ca^{2+} release events later visualized directly in guinea pig ileal myocytes using confocal microscopy (Gordienko et al., 1998). These foundational studies established that small intestinal STOCs couple RyR-mediated Ca^{2+} release to BK channel activation (Bolton & Imaizumi, 1996) but left two critical questions unanswered: what triggers spontaneous RyR opening in these cells, and how does the spark-STOC pathway connect to functional motility outcomes?

In vascular smooth muscle both answers are clear: Ca^{2+} entry through L-type voltage-gated channels refills SR stores and provides the CICR trigger for RyR-mediated sparks, and BK β1-subunits confer sufficient Ca^{2+} sensitivity for spark-STOC coupling to regulate myogenic tone (Dopico et al., 2018; Jaggar et al., 2000; Takeda et al., 2011). However although the small intestinal RyR-BK

axis was established pharmacologically decades ago, the upstream trigger that initiates RyR-dependent Ca^{2+} release remained undefined, suggesting an alternative, potentially mechanosensitive mechanism.

Our study provides the structural basis for the distribution of Piezo1 in small intestinal SMC and its organization with RyRs and BK channels. We found that intra-Piezo1 and RyR clusters reside intracellularly, with enrichment of intra-Piezo1-RyR colocalization in intracellular domains. Intra-Piezo1 is in proximity to both RyR and BK_{Ca} channels within <40 nm, with a greater abundance of intra-Piezo1-BK_{Ca} puncta, suggesting that multiple BK_{Ca} channels likely surround intra-Piezo1-RyR release sites, recapitulating the amplification logic of vascular spark-STOC coupling while adding a mechanosensitive trigger to the triad (Brenner et al., 2000; Plüger et al., 2000).

Physiological consequences: the molecular brake on GI motility

Piezo1 activation with Yoda2 slowed force development, whereas the relaxation phase was relatively preserved despite an overall 57% reduction in amplitude (Fig. 1*D*). This asymmetry is consistent with BK_{Ca}-mediated hyperpolarization reducing voltage-gated Ca^{2+} channel activity (Hill-Eubanks et al., 2011; Nelson et al., 1995), which would blunt Ca^{2+}-dependent myosin light-chain phosphorylation and slow force generation, while leaving SERCA-mediated Ca^{2+} reuptake and myosin phosphatase activity, the principal drivers of relaxation, unaffected (Hill-Eubanks et al., 2011). The brake induced by Yoda2-mediated Piezo1 activation thus appears to act selectively on excitation–contraction coupling rather than globally suppressing the contractile cycle. The 152% increase in period variability, accompanied by only a small reduction in frequency, may reflect a direct effect on ICC pacemaker activity or an indirect effect mediated by other cell types (Sanders et al., 2023; Won et al., 2005).

The mechanotransduction brake in smooth muscle demonstrated in this study may contribute to intestinal peristaltic co-ordination. Luminal distension stretches the circular smooth muscle layer, activating SR-resident Piezo1 and triggering Ca^{2+} sparks, BK_{Ca}-mediated STOCs and membrane hyperpolarization, ensuring that the muscle segment remains relaxed and preventing excessive wall tension that could obstruct flow. As the bolus advances decreasing wall tension would reduce Piezo1 activation and release the brake, allowing excitatory inputs from interstitial cells of Cajal and enteric neurons to drive contraction (Sanders et al., 2023). If correct, the spatial gradient of mechanical stimulation would create a corresponding gradient of brake engagement: strongly engaged in the distended receiving region, then progressively less engaged upstream, producing the co-ordinated relaxation–contraction wave characteristic of peristalsis.

This model extends the 'mechanical brakes' concept presented in Joshi et al. (2021), with our data providing a candidate molecular architecture: a Piezo1-RyR-BK_{Ca} complex whose brake strength could scale with junction density and mechanical strain. The prediction is testable: loss of the brake should disrupt co-ordinated mechano-relaxation, and our previous Piezo1-deficient mice show impaired transit and altered faecal pellet characteristics (Bautista et al., 2025), consistent with, though not proof of, this mechanism. Direct demonstration would require measuring Piezo1-dependent BK_{Ca} currents in response to physiological stretch rather than pharmacological activation. Furthermore our PLA quantification revealed that the density of the Piezo1-RyR-BK_{Ca} complex varies by more than an order of magnitude across individual cells. This variability suggests that these junctions are highly dynamic, actively trafficked by the cytoskeleton in response to mechanical demand, much like the junctional SR motility observed in cardiac myocytes (Drum et al., 2020). Consistent with a dynamically regulated junction both the Piezo1-BK_{Ca} colocalization signal and the BK_{Ca} dependence of Piezo1-evoked relaxation are increased in mesenteric artery smooth muscle from type 2 diabetic mice relative to controls (Haam et al., 2024), indicating that the density of this coupling is set by physiological state rather than fixed.

Limitations and future directions

Several limitations bound our interpretation. Because Yoda2 is membrane permeant, the responses we report reflect the combined activity of plasma membrane and intracellular Piezo1, and the agonists used to bias activation towards the surface pool are not fully selective. Sex-disaggregated analysis of contractility was extended to all nine parameters and revealed that baseline contraction and relaxation velocities were faster in males ($P = 0.00148$ and $P = 0.00417$), whereas amplitude, force and frequency were indistinguishable between sexes. This suggests possible sex differences in excitation–contraction kinetics, such as SR Ca^{2+} handling, myosin phosphatase activity or interstitial cell of Cajal pacemaker functions. Due to unequal group sizes and the lack of prior power analysis for sex we consider this a hypothesis-generating observation and a specific target for future research.

In intact tissue the persistence of Yoda2-mediated inhibition after SERCA blockade indicates that non-muscle elements contribute to the response, so the wire myography experiments alone cannot support strong mechanistic conclusions. The ryanodine experiments face

similar limitations: at the concentration used the near loss of baseline contractility complicates distinguishing between the absence of a Yoda2 effect and a floor effect. However not all preparations exhibited such a severe reduction in contractions, indicating that the tissue likely remained viable. Our imaging indicates that Piezo1 is situated within nanoscale proximity to RyR and BKCa. This observation aligns with the presumption of its residence on the SR membrane; however it does not definitively establish this. The precise configuration of Piezo1, RyR and BKCa as reported requires independent verification in smooth muscle tissue.

The concentration of Jedi2 used in this study (200 μM) approximates the published EC_{50} of ∼158 μM for mouse Piezo1 determined in a cell-based calcium flux assay (Wang et al., 2018) and is therefore expected to produce submaximal but physiologically meaningful activation of PM-Piezo1. However the EC_{50} determined in heterologous expression systems may not directly translate to intact tissue, where diffusion barriers, extracellular matrix interactions and differences in channel density could alter effective drug concentrations. A full Jedi2 dose–response in intestinal muscularis, extended to higher concentrations for Piezo1 activation (Wang et al., 2018), is needed for a more complete assessment of PM Piezo1's role in contractile regulation and is an important future direction.

The principal question that remains open is whether the Ca^{2+} that activates BK_{Ca} arises from SR-localized Piezo1 or from surface Piezo1 acting through secondary calcium-induced calcium release, a distinction that conventional cytoplasmic indicators cannot resolve. Future work in our laboratory will address this using compartment-targeted genetically encoded Ca^{2+} sensors and stretch-evoked rather than pharmacological activation, together with a full Jedi2 and GsMTx4 dose–response characterization in intestinal tissue. Assessing whether the loss of the Piezo1-RyR-BKCa complex disrupts co-ordinated mechano-relaxation will be essential to connect this architecture to peristaltic behaviour and its significance in gut motility.

Conclusion

These findings extend mechanotransduction in the GI tract beyond the cell surface. Piezo1 is not solely a surface portal for excitation; it also acts as a sensor that confers mechanosensitivity on an intracellular compartment. By recruiting RyR and BK_{Ca} channels into a nanoscale signalling hub intra-Piezo1 forms a feedback loop that tunes excitability from within the cell, supporting the regulated motility the intestine requires.

APPENDIX

Supporting statistical tables and source data for 'Intracellular Mechanosensation in Intestinal Smooth Muscle: Piezo1 Complexes Amplify Signalling Beyond the Surface' (Tables A1–A7). Values are presented as mean ± SD; N = animals (mice), n = cells, segments or preparations as indicated.

Table A1. Sex-disaggregated analysis of contractility data

Parameter	Sex	*N*	Baseline	Yoda2	Change	Sex effect *P*	Result
Amplitude (mN)	M	5	0.3083 ± 0.1298	0.1400 ± 0.0528	−0.1683 ± 0.0860	Sex $P = 0.661$; interaction $P = 0.955$	No sex effect
	F	7	0.2899 ± 0.1004	0.1187 ± 0.0369	−0.1712 ± 0.0818		
Integral force (mN·s)	M	5	17.2840 ± 5.9702	8.3340 ± 3.2281	−8.9500 ± 3.1402	Sex $P = 0.994$; interaction $P = 0.391$	No sex effect
	F	7	18.2757 ± 5.6381	7.3771 ± 2.5326	−10.8986 ± 4.0586		
Frequency (cpm)	M	5	30.9208 ± 1.3237	29.8008 ± 2.1261	−1.1200 ± 2.9347	Sex $P = 0.907$; interaction $P = 0.222$	No sex effect
	F	7	32.2009 ± 4.5182	27.8863 ± 7.6000	−4.3145 ± 4.8481		
Period CV (%)	M	5	10.4803 ± 5.9083	26.3570 ± 9.2838	+15.8767 ± 11.3631	Sex $P = 0.659$; interaction $P = 0.855$	No sex effect
	F	7	9.1320 ± 6.3642	23.1026 ± 19.4408	+13.9705 ± 20.3455		
Duration (s)	M	5	1.4974 ± 0.2606	1.6741 ± 0.0993	+0.1767 ± 0.2053	Sex $P = 0.401$; interaction $P = 0.835$	No sex effect
	F	7	1.5944 ± 0.1452	1.7473 ± 0.2201	+0.1529 ± 0.1791		
d*F*/d*t* max (mN/s)	M	5	4.0461 ± 0.2966	3.5073 ± 0.3356	−0.5388 ± 0.3704	Sex $P = 0.00148$; interaction $P = 0.715$	Sex effect: M > F
	F	7	3.0264 ± 0.5801	2.5736 ± 0.3879	−0.4528 ± 0.4040		
Time to peak (s)	M	5	0.7420 ± 0.1152	0.9100 ± 0.0453	+0.1680 ± 0.0931	Sex $P = 0.589$; interaction $P = 0.346$	No sex effect
	F	7	0.8000 ± 0.1085	0.9014 ± 0.0930	+0.1014 ± 0.1246		
Time from peak (s)	M	5	0.6760 ± 0.0527	0.6360 ± 0.0344	−0.0400 ± 0.0745	Sex $P = 0.154$; interaction $P = 0.813$	No sex effect
	F	7	0.7557 ± 0.1119	0.7014 ± 0.1099	−0.0543 ± 0.0873		
d*F*/d*t* min (mN/s)	M	5	−3.7321 ± 0.2909	−3.4367 ± 0.3924	+0.2955 ± 0.5618	Sex $P = 0.00417$; interaction $P = 0.758$	Sex effect: M > F
	F	7	−2.9332 ± 0.6055	−2.5519 ± 0.3990	+0.3813 ± 0.3838		

Note: Values are presented as mean ± SD. Sex differences were assessed using mixed-model two-way repeated-measures ANOVA (treatment as within-subject factor, sex as between-subject factor). The sex effect *P*-value reflects the main effect of sex collapsed across treatment conditions. No sex × treatment interaction was significant for any parameter (interaction *P*-values reported per-parameter above), justifying pooled analysis of the treatment effect. Sex main effects were detected for d*F*/d*t* max ($P = 0.00148$) and d*F*/d*t* min ($P = 0.00417$), both faster in males; no other parameter showed a sex main effect. $N = 12$ mice (5 males and 7 females).

Table A2. Yoda2 amplitude dose–response in intact small intestine

Yoda2 (μM)	*N* mice	Baseline amplitude (mN)	+Yoda2 amplitude (mN)	Amplitude (% of baseline)
1	2	0.1806 ± 0.0224	0.1354 ± 0.0184	76.2157 ± 19.6604
5	3	0.1653 ± 0.0274	0.1403 ± 0.0221	86.7054 ± 21.6370
10	2	0.1925 ± 0.1232	0.1606 ± 0.0654	91.2495 ± 24.3937
25	12	0.2976 ± 0.1082	0.1276 ± 0.0427	44.1262 ± 10.4364

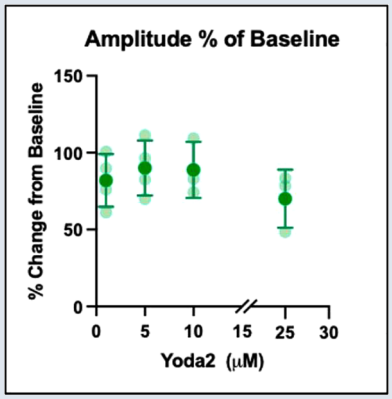

Note: Within-tissue paired design: contraction amplitude measured at baseline and after a single Yoda2 concentration in each mouse; amplitude as percentage of baseline is the within-mouse ratio. Values are presented as mean ± SD. *N* = mice. Approximate one-site inhibition fit (Yoda2 only, anchored on the full 25 μM dataset): $IC_{50} \approx 22.6$ μM (95% confidence interval (CI): 14.2–30.9 μM; $R^2 = 0.53$); the 1–10 μM points are *N* = 2–3 mice, so the curve below 25 μM is approximate.

Table A3. Contractile parameters during membrane-impermeant pharmacological dissection of surface *versus* intracellular Piezo1 (Figure 2)

Section A: GsMTx4 (2.5 μM), $N = 5$ mice					
Parameter	Baseline	+GsMTx4	GsMTx4 + Y2	Omnibus test	Displayed comparison (*P*)
Amplitude (mN)	0.1672 ± 0.0389	0.1987 ± 0.0846	0.0888 ± 0.0542	RM one-way ANOVA $F(1.4097, 5.6390) = 9.9851$, $P = 0.0173$	Baseline *vs.* +Yoda2: $P = 0.0427$ (Holm–Šídák)
Integral Force (mN·s)	11.5596 ± 2.3511	12.3158 ± 4.4705	6.1309 ± 2.2858	RM one-way ANOVA $F(1.3172, 5.2690) = 9.3516$, $P = 0.0229$	Baseline *vs.* +Yoda2: $P = 0.0181$; +GsMTx4 *vs.* +Yoda2: $P = 0.0731$ (Holm–Šídák)
Frequency (cpm)	29.6802 ± 2.3562	28.2002 ± 8.1731	24.2002 ± 13.1363	Friedman statistic = 3.4444, $P = 0.185$	Not significant; no comparison displayed
Section B: Jedi2 (200 μM), $N = 5$ mice					
Parameter	Baseline	+Jedi2	Jedi2 + Y2	Omnibus test	Displayed comparison (*P*)
Amplitude (mN)	0.1752 ± 0.0578	0.1711 ± 0.0918	0.0949 ± 0.0568	RM one-way ANOVA $F(1.1505, 4.6019) = 7.0407$, $P = 0.0472$	Baseline *vs.* +Yoda2: $P = 0.0421$ (Holm–Šídák)
Integral force (mN·s)	11.6340 ± 1.6862	12.1418 ± 1.9630	6.4241 ± 1.7067	Friedman's statistic = 7.6000, $P = 0.0239$	+Jedi2 *vs.* +Yoda2: $P = 0.0342$ (Dunn's test)
Frequency (cpm)	32.6005 ± 1.7378	30.8405 ± 1.7969	27.0404 ± 5.9521	Friedman's statistic = 7.6842, $P = 0.0185$	Baseline *vs.* +Yoda2: $P = 0.0216$ (Dunn's test)

Note: Values are presented as animal-averaged mean ± SD; $N = 5$ mice per tool. All usable recordings from an animal were averaged to a single animal value before analysis; the number of usable recordings varied between animals. Each segment was tested at one concentration only followed by Yoda2 (25 μM). Omnibus tests and the displayed *post hoc* comparisons are listed per parameter; comparisons not shown were not significant.
Abbreviation: RM, repeated measures.

Table A4. Contractile parameters during pharmacological SR Ca^{2+} store disruption

Section A: Thapsigargin (10 μM), $N = 9$ mice (4M/5F)						
Parameter	Baseline	+TG	TG + Y2	*P* (B–drug)	*P* (drug–Y2)	RM ANOVA
Amplitude (mN)	0.304 ± 0.111	0.141 ± 0.065	0.094 ± 0.059	0.00539	0.00613	$F(1.172, 9.373) = 23.99$ $P = 0.000561$
Integral force (mN·s)	18.14 ± 5.39	8.90 ± 3.82	6.37 ± 4.56	0.00182	0.0133	$F(1.215, 9.717) = 27.81$ $P = 0.000266$
Frequency (cpm)	31.15 ± 2.60	24.00 ± 7.50	11.07 ± 7.64	0.0253	0.00451	$F(1.909, 15.27) = 29.09$ $P = 7.30 \times 10^{-6}$
Section B: Ryanodine (100 μM), $N = 10$ mice (5M/5F)						
Parameter	Baseline	+Ry	Ry + Y2	*P* (B–drug)	*P* (drug–Y2)	RM ANOVA
Amplitude (mN)	0.264 ± 0.086	0.102 ± 0.052	0.115 ± 0.083	0.000693	1.000	Friedman's statistic = 15.20 $P = 8.54 \times 10^{-5}$
Integral force (mN·s)	16.74 ± 5.94	6.557 ± 3.18	6.741 ± 4.31	4.88×10^{-5}	0.803	$F(1.403, 12.63) = 48.46$ $P = 3.77 \times 10^{-6}$
Frequency (cpm)	31.70 ± 3.43	15.76 ± 10.87	14.52 ± 9.79	0.00229	0.542	$F(1.516, 13.64) = 20.95$ $P = 0.000151$

Note: Values are presented as animal-averaged mean ± SD. Repeated-measures one-way ANOVA with Geisser-Greenhouse correction, except ryanodine amplitude, which failed the Shapiro-Wilk normality test and was analysed using Friedman's test. Post hoc Holm–Šídák or Dunn's test for the Friedman analysis, with two planned comparisons per parameter (baseline *vs*. drug; drug *vs*. drug + Y2). Adjusted *P*-values are reported.

Abbreviations: B, baseline; cpm, contractions per minute; RM, repeated measures; Ry, ryanodine; TG, thapsigargin; Y2, Yoda2 (25 μM).

Table A5. Whole-cell patch-clamp statistical analysis

Section A: Paired *t* test conditions (panels 4*B* and 4*D*)

Panels	Condition	*N*	*n*	Baseline (pA/pF)	+Y2 (pA/pF)	Test	*t*-statistic	*P*-value	Cohen's *d*
4*B*	Yoda2 (10 μM) only	7	18	−0.30 ± 0.36	2.49 ± 1.81	Paired *t* test	t(6) = 5.50	0.00151	2.0788
4*D*	Thapsigargin pretreatment (1 μM)	5	7	−0.30 ± 0.34	−0.06 ± 0.33	Paired *t* test	*t*(4) = 1.693	0.166	0.7571

Section B: RM ANOVA with paxilline blockade (panels 4*F* and 4*H*)

Panel	Condition	*N*	*n*	Baseline (pA/pF)	+Y2 (pA/pF)	Y2 + Px (pA/pF)	*P* (B–Y2)	*P* (Y2–Px)	RM ANOVA
4F	$[1.8\ mM\ Ca^{2+}]_o$ Yoda2 (10 μM) + paxilline (10 μM)	6	10	−0.23 ± 0.33	2.83 ± 1.39	1.04 ± 0.71	0.00779	0.00346	$F(1.02, 5.11) = 25.57$ $P = 0.00362$
4H	$[0\ mM\ Ca^{2+}]_o$ Yoda2 (10 μM) + paxilline (10 μM)	3	3	−0.11 ± 0.19	4.82 ± 1.18	2.15 ± 0.61	0.00200	0.0192	$F(2, 4) = 37.18$ $P = 0.00261$

Note: Values are presented as mean ± SD of animal-averaged data. Paired *t* tests on per-animal means. Repeated measures one-way ANOVA with Geisser-Greenhouse correction; Bonferroni's *post hoc*. *N* = animals; *n* = individual cells. Cohen's *d* = mean difference/SD of differences. Per-animal averages are used. SD values are verified against Prism descriptive statistics output.

Abbreviations: Px, paxilline (10 μM); RM, repeated measures; Y2, Yoda2 (10 μM).

Table A6. Subcellular localization of Piezo1 and associated channels: ICC and PLA statistics

Section A: subcellular compartment distribution (panels 5*E–H*)

Panel	Measurement	Compartment	Sex	Mean ± SD	*N*	*n*	Test	Statistics
5E	Piezo1 % compartment	Intracellular	M	86.30 ± 7.89	5	23	Compartment: paired *t* test on per-animal means; sex: see Statistics	Compartment: $t(9) = 21.98$, $P = 3.94 \times 10^{-9}$
		Intracellular	F	86.02 ± 6.82	5	25		Sex: $t(4.44) = 0.245$, $P = 0.818$
		Plasma membrane	M	13.70 ± 7.89	5	23		Sex × Comp: not estimable
		Plasma membrane	F	13.98 ± 6.82	5	25		
5F	RyR % compartment	Intracellular	M	80.76 ± 9.54	5	23	Compartment: paired *t* test on per-animal means; sex: see Statistics	Compartment: $t(9) = 17.64$, $P = 2.74 \times 10^{-8}$
		Intracellular	F	80.89 ± 9.22	5	25		Sex: $t(4.82) = 0.348$, $P = 0.743$
		Plasma membrane	M	19.28 ± 9.58	5	23		Sex × Comp: not estimable
		Plasma membrane	F	19.11 ± 9.22	5	25		
5G	# Colocalization foci	Intracellular	M	108.87 ± 29.05	5	23	Compartment: paired *t* test on per-animal means; sex: see Statistics	Compartment: $t(9) = 13.50$, $P = 2.80 \times 10^{-7}$
		Intracellular	F	118.80 ± 41.38	5	25		Sex: $U = 9$, $P = 0.548$
		Plasma membrane	M	19.61 ± 16.34	5	23		Sex × Comp: $F(1,8) = 0.385$, $P = 0.552$
		Plasma membrane	F	23.28 ± 17.29	5	25		
5H	% Colocalization	Intracellular	M	10.08 ± 2.78	5	23	Compartment: paired *t* test on per-animal means; sex: see Statistics	Compartment: $t(9) = 14.47$, $P = 1.54 \times 10^{-7}$
		Intracellular	F	10.69 ± 3.69	5	25		Sex: $t(6.38) = 0.129$, $P = 0.901$
		Plasma membrane	M	1.80 ± 1.43	5	23		Sex × Comp: $F(1,8) = 0.341$, $P = 0.575$
		Plasma membrane	F	2.02 ± 1.39	5	25		

(*Continued*)

Table A6. (Continued)

Section B: proximity ligation assay (PLA) statistics (panels 6*C–E*)

Panel	PLA pair	Mean puncta/mm^2	Control/comparison	*N* mice	Test	*P*-value 1	*P*-value 2
6C	RyR2–Piezo1	81.49 ± 40.44	0.43 / 4.15 (ctrls)	11	Ordinary one-way ANOVA (Holm–Šídák) ($P = 0.0109$)	0.0288	0.0288
6D	BK_{Ca}–Piezo1	161.82 ± 80.35	1.78 / 4.15 (ctrls)	12	Ordinary one-way ANOVA (Holm–Šídák) ($P = 0.00896$)	0.0280	0.0280
6E	BK_{Ca} *vs.* RyR2	161.82 ± 80.35 *vs.* 81.49 ± 40.44	BK_{Ca}–Piezo1 *vs.* RyR2–Piezo1	12 *vs.* 11	Welch's *t* test	0.00718	—

Note: Values are presented as mean ± SD computed across cells ($n = 23$ males and 25 females; 48 total); all inferential tests were performed on per-animal means ($N = 5$ animals per sex, 10 total). Compartment effects were tested using paired *t* test on per-animal means (d$F = 9$). Sex was tested by comparing the plasma membrane value between sexes ($N = 5$ *vs.* 5). Normality was assessed within each sex using the Shapiro-Wilk test; only the male group of panel 5*G* departed from normality ($W = 0.709$, $P = 0.0119$), so that panel was analysed using Mann–Whitney and the remaining panels using unpaired *t* test with Welch's correction, which was applied throughout because the *F* test indicated unequal variances for panels 5*E* ($F(4,4) = 17.97$, $P = 0.0161$) and 5*F* ($F(4,4) = 9.63$, $P = 0.0497$). No sex effect reached significance for any parameter. For panels 5*E* and 5*F* the plasma membrane and intracellular values are complementary fractions of the same cluster population and sum to 100%, so between-animal variance in the subject means is zero by construction, and a sex × compartment interaction is not estimable; for these panels the sex effect on the membrane fraction fully determines the effect on the intracellular fraction.

Abbreviations: ctrl, control; Intra, intracellular compartment; PM, plasma membrane

Note: Values are presented as mean ± SD across animals; *N* = mice. Each per-animal value is the mean of all PLA images from that animal, so the SD reflects animal-to-animal variation, matching the unit of the inferential tests. Panels 6*C* and 6*D* were analysed using ordinary one-way ANOVA on per-animal means with Holm–Šídák *post hoc*, comparing each PLA pair against its two single-antibody controls. *P*-value 1 and *P*-value 2 are the comparisons against the two single-antibody controls (target protein alone and Piezo1 alone), which together constitute the specificity test; the control column lists their mean puncta densities. Panel 6*E* compares BK_{Ca}-Piezo1 ($N = 12$) and RyR-Piezo1 ($N = 11$) puncta density directly by Welch's unpaired *t* test (unequal variances, variance-ratio *F* test $P = 0.0389$).

Table A7. Antibodies, reagents, chemicals and software source data

Section A: primary and secondary antibodies

Antigen target	Company	Catalogue #, Lot #	Dilution (Exp)	RRID #
Piezo1 (rabbit)	Alomone Labs	APC-087 APC087AN0902	1:100 (ICC); 1:200 (PLA)	AB_2756743
RyR2 (mouse)	Thermo Fisher Scientific (Waltham, MA, USA)	MA3-916, ZA389382	1:50 (ICC); 1:200 (PLA)	AB_2183054
RFP (chicken)	Rockland	600-901-379	1:100 (ICC)	AB_10704808
BKα/Slo1 (mouse)	Neuromab	75-022, 472-2JU-03	1:200 (PLA)	AB_2249538
WGA-Alexa Fluor 488	Thermo Fisher Scientific (Waltham, MA, USA)	W11261, 2 789 910	5 µg/mL (ICC)	AB_2 651 016
Alexa Fluor 568 goat anti-chicken IgY	Thermo Fisher Scientific (Waltham, MA, USA)	A-11 041, 2 674 372	1:1000 (ICC)	AB_2534 098
Cyanine5 goat anti-mouse IgG	Thermo Fisher Scientific (Waltham, MA, USA)	A10524, 2 720 381	1:1000 (ICC)	AB_10562712

Section B: reagents and pharmacological agents

Reagent	Company	Catalogue #	Final Conc. (Exp)
Yoda2	Sigma–Aldrich	SML3910	25 µM (wire myography); 10 µM (patch clamp)
Thapsigargin	Fisher Scientific	11-381	10 µM (wire myography); 1 µM (patch clamp)
Ryanodine	Abcam	ab120083	100 µM (wire myography)
Paxilline	Tocris Bioscience	2006	10 µM (patch clamp)
Collagenase Type II	Worthington	LS004176	2.0 mg/mL (SMC isolation)
Trypsin inhibitor	Worthington	52P23070	1.0 mg/mL (SMC isolation)
Papain	Thermo Fisher Scientific (Waltham, MA, USA)	416 761 000	0.5 mg/mL (SMC isolation)
DL-Dithiothreitol	Sigma–Aldrich	D9163-1G	154.25 µM (SMC isolation)
Adenosine 5′-triphosphate Mg^{2+} salt	Sigma–Aldrich	A9187-1G	0.27 mg/mL (SMC isolation)
Bovine serum albumin	Sigma–Aldrich	A9418-100G	1–2 mg/mL (SMC isolation)

Section C: software

Software	Identifier/source
LabChart 8	ADInstruments; https://www.adinstruments.com/products/labchart
GraphPad Prism 10	GraphPad Software; https://www.graphpad.com
Wire Myography Analyzer	https://doi.org/10.5281/zenodo.18472624
Imaris 10	Oxford Instruments; https://imaris.oxinst.com

Abbreviations: ExP, experimental application; ICC, immunofluorescence; Patch, patch-clamp electrophysiology; PLA, proximity ligation assay; SMC, smooth muscle cell; Wire, wire myography. (,) indicates catalogue number not available in source document.

References

Alcaino, C., Farrugia, G., & Beyder, A. (2017). Mechanosensitive piezo channels in the gastrointestinal tract. *Current Topics in Membranes*, **79**, 219–244.

Alper, S. L. (2017). Genetic diseases of PIEZO1 and PIEZO2 dysfunction. *Current Topics in Membranes*, **79**, 97–134.

Bae, C., Sachs, F., & Gottlieb, P. A. (2011). The mechanosensitive ion channel Piezo1 is inhibited by the peptide GsMTx4. *Biochemistry*, **50**(29), 6295–6300.

Bautista, G. M., Du, Y., Matthews, M. J., Flores, A. M., Kushnir, N. R., Sweeney, N. K., Nguyen, N. P. N., Tokhtaeva, E., Solorzano-Vargas, R. S., Lewis, M., Stelzner, M., He, X., Dunn, J. C. Y., & Martin, M. G. (2025). Smooth muscle cell Piezo1 depletion results in impaired contractile properties in murine small bowel. *Communications Biology*, **8**(1), 448.

Bautista, G. M., Santana, L. F., & Martin, M. G. (2026). Piezo1 in intestinal smooth muscle cells: Emerging perspectives. *The Journal of Physiology*, **604**(1), 129–144.

Bayguinov, O., Hagen, B., Bonev, A. D., Nelson, M. T., & Sanders, K. M. (2000). Intracellular calcium events activated by ATP in murine colonic myocytes. *American Journal of Physiology-Cell Physiology*, **279**(1), C126–C135.

Bayguinov, O., Hagen, B., & Sanders, K. M. (2001). Muscarinic stimulation increases basal Ca(2+) and inhibits spontaneous Ca^{2+} transients in murine colonic myocytes. *American Journal of Physiology-Cell Physiology*, **280**(3), C689–C700.

Benham, C. D., Bolton, T. B., Lang, R. J., & Takewaki, T. (1986). Calcium-activated potassium channels in single smooth muscle cells of rabbit jejunum and guinea-pig mesenteric artery. *The Journal of Physiology*, **371**(1), 45–67.

Berrier, C., Pozza, A., de Lacroix de Lavalette, A., Chardonnet, S., Mesneau, A., Jaxel, C., le Maire, M., & Ghazi, A. (2013). The purified mechanosensitive channel TREK-1 is directly sensitive to membrane tension. *Journal of Biological Chemistry*, **288**(38), 27307–27314.

Bolton, T. B., & Imaizumi, Y. (1996). Spontaneous transient outward currents in smooth muscle cells. *Cell Calcium*, **20**(2), 141–152.

Bolton, T. B., & Lim, S. P. (1989). Properties of calcium stores and transient outward currents in single smooth muscle cells of rabbit intestine. *The Journal of Physiology*, **409**(1), 385–401.

Brenner, R., Peréz, G. J., Bonev, A. D., Eckman, D. M., Kosek, J. C., Wiler, S. W., Patterson, A. J., Nelson, M. T., & Aldrich, R. W. (2000). Vasoregulation by the beta1 subunit of the calcium-activated potassium channel. *Nature*, **407**(6806), 870–876.

Carrisoza-Gaytan, R., Mutchler, S. M., Carattino, F., Soong, J., Dalghi, M. G., Wu, P., Wang, W., Apodaca, G., Satlin, L. M., & Kleyman, T. R. (2024). PIEZO1 is a distal nephron mechanosensor and is required for flow-induced K+ secretion. *Journal of Clinical Investigation* **134**(5), e174806.

Chen, B., Wang, J., Qian, Q., Zhang, G., Wang, Y., Li, M., Tan, R., Yang, Z., Zhao, W., Ciampa, G., Yang Bennett, D. S., Liu, Y., Zhu, Q.i, Zhu, Z., Masenga, S. K., Vue, Z., Le, H., Shi, Q., Zingman, L. V., … Song, L.-S. (2026). Junctophilin-2-orchestrated calcium signalosome regulates brown adipocyte thermogenesis and energy metabolism. *Proceedings of the National Academy of Sciences of the United States of America*, **123**(27), e2524943123.

Collier, M. L., Ji, G., Wang, Y.-X., & Kotlikoff, M. I. (2000). Calcium-induced Calcium release in smooth muscle: Loose coupling between the action potential and Calcium release. *Journal of General Physiology*, **115**(5), 653–662.

Coste, B., Mathur, J., Schmidt, M., Earley, T. J., Ranade, S., Petrus, M. J., Dubin, A. E., & Patapoutian, A. (2010). Piezo1 and Piezo2 are essential components of distinct mechanically activated cation channels. *Science*, **330**(6000), 55–60.

Dopico, A. M., Bukiya, A. N., & Jaggar, J. H. (2018). Calcium- and voltage-gated BK channels in vascular smooth muscle. *Pflugers Archiv: European Journal of Physiology*, **470**(9), 1271–1289.

Drum, B. M., Yuan, C., de la Mata, A., Grainger, N., & Santana, L. F. (2020). Junctional sarcoplasmic reticulum motility in adult mouse ventricular myocytes. *American Journal of Physiology-Cell Physiology*, **318**(3), C598–C604.

Earley, S. (2013). Smooth muscle cell ca^{2+}: Think locally, act globally. *Microcirculation*, **20**(4), 279–280.

Erdogan, B. R., Karaomerlioglu, I., Yesilyurt, Z. E., Ozturk, N., Muderrisoglu, A. E., Michel, M. C., & Arioglu-Inan, E. (2020). Normalization of organ bath contraction data for tissue specimen size: Does one approach fit all? *Naunyn-Schmiedebergs Archives of Pharmacology*, **393**(2), 243–251.

Gnanasambandam, R., Bae, C., Gottlieb, P. A., & Sachs, F. (2015). Ionic selectivity and permeation properties of Human PIEZO1 channels. *PLOS ONE*, **10**(5), e0125503.

Gnanasambandam, R., Ghatak, C., Yasmann, A., Nishizawa, K., Sachs, F., Ladokhin, A. S., Sukharev, S. I., & Suchyna, T. M. (2017). GsMTx4: Mechanism of inhibiting mechanosensitive ion channels. *Biophysical Journal*, **112**(1), 31–45.

Gollasch, M., Wellman, G. C., Knot, H. J., Jaggar, J. H., Damon, D. H., Bonev, A. D., & Nelson, M. T. (1998). Ontogeny of local sarcoplasmic reticulum Ca2+ signals in cerebral arteries: Ca2+ sparks as elementary physiological events. *Circulation Research*, **83**(11), 1104–1114.

Gonzalez-Cobos, J., C. (2010). TRPC channels in smooth muscle cells. *Frontiers in Bioscience (Landmark Edition)*, **15**(3), 1023–1039.

Gordienko, D. V., Bolton, T. B., & Cannell, M. B. (1998). Variability in spontaneous subcellular calcium release in guinea-pig ileum smooth muscle cells. *The Journal of Physiology*, **507**(Pt 3), 707–720.

Gu, Y., & Gu, C. (2014). Physiological and pathological functions of mechanosensitive ion channels. *Molecular Neurobiology*, **50**(2), 339–347.

Gudipaty, S. A., Lindblom, J., Loftus, P. D., Redd, M. J., Edes, K., Davey, C. F., Krishnegowda, V., & Rosenblatt, J. (2017). Mechanical stretch triggers rapid epithelial cell division through Piezo1. *Nature*, **543**(7643), 118–121.

Guntur, D., Jeremic, D., Csaki, R., Myronenko, O., Biasin, V., Kolb, D., Michalick, L., Kuebler, W. M., Enyedi, P., Olschewski, H., Olschewski, A., & Nagaraj, C. (2025). BK channels are indispensable for endothelial function in small pulmonary arteries. *Cell Communication and Signaling*, **23**(1), 448.

Guo, Y. R., & MacKinnon, R. (2017). Structure-based membrane dome mechanism for Piezo mechanosensitivity. *eLife*, **6**, e33660.

Haam, C. E., Choi, S., Byeon, S., Oh, E. Y., Choi, S. K., & Lee, Y. H. (2024). Alteration of Piezo1 signaling in type 2 diabetic mice: Focus on endothelium and BK_{Ca} channel. *Pflugers Archiv: European Journal of Physiology*, **476**(10), 1479–1492.

Hill-Eubanks, D. C., Werner, M. E., Heppner, T. J., & Nelson, M. T. (2011). Calcium signaling in smooth muscle. *Cold Spring Harbor Perspectives in biology*, **3**(9), a004549.

Huang, H., Kamm, R. D., & Lee, R. T. (2004). Cell mechanics and mechanotransduction: Pathways, probes, and physiology. *American Journal of Physiology-Cell Physiology*, **287**(1), C1–C11.

Jaggar, J. H., Porter, V. A., Lederer, W. J., & Nelson, M. T. (2000). Calcium sparks in smooth muscle. *American Journal of Physiology-Cell Physiology*, **278**(2), C235–C256.

Joshi, V., Strege, P. R., Farrugia, G., & Beyder, A. (2021). Mechanotransduction in gastrointestinal smooth muscle cells: Role of mechanosensitive ion channels. *American Journal of Physiology Gastrointestinal and Liver Physiology*, **320**(5), G897–G906.

Koh, S. D., Bradley, K. K., Rae, M. G., Keef, K. D., Horowitz, B., & Sanders, K. M. (1998). Basal activation of ATP-sensitive potassium channels in murine colonic smooth muscle cell. *Biophysical Journal*, **75**(4), 1793–1800.

Kotlikoff, M. I. (2003). Calcium-induced calcium release in smooth muscle: The case for loose coupling. *Progress in Biophysics and Molecular Biology*, **83**(3), 171–191.

Lewis, A. H., Cronin, M. E., & Grandl, J. (2024). Piezo1 ion channels are capable of conformational signaling. *Neuron*, **112**(18), 3161–3175e5.

Liao, J., Lu, W., Chen, Y., Duan, X., Zhang, C., Luo, X., Lin, Z., Chen, J., Liu, S., Yan, H., Chen, Y., Feng, H., Zhou, D., Chen, X., Zhang, Z., Yang, Q., Liu, X., Tang, H., Li, J., … Wang, J. (2021). Upregulation of Piezo1 (Piezo Type Mechanosensitive Ion Channel Component 1) enhances the intracellular free calcium in pulmonary arterial smooth muscle cells from idiopathic pulmonary arterial hypertension patients. *Hypertension*, **77**(6), 1974–1989.

Lim, X. R., & Harraz, O. F. (2024). Mechanosensing by vascular endothelium. *Annual Review of Physiology*, **86**(1), 71–97.

Liu, Y., Song, Y., Ren, X., Li, M., Liu, S., Li, Z., Ding, D., & Lu, X. (2026). Piezo1-mediated neuroexcitation via collaboration with KCa1.1 and Nav1.9 currents in myelinated ah-type of trigeminal ganglion neurons in rats: Mechanistic insights with sex-specific effects. *Molecular Pain*, **22**, 17448069251410754.

Lytton, J., Westlin, M., & Hanley, M. R. (1991). Thapsigargin inhibits the sarcoplasmic or endoplasmic reticulum Ca-ATPase family of calcium pumps. *Journal of Biological Chemistry*, **266**(26), 17067–17071.

Martín-Aragón Baudel, M, Flores-Tamez, V. A., Hong, J., Reddy, G. R., Maillard, P., Burns, A. E., Man, K. N. M., Sasse, K. C., Ward, S. M., Catterall, W. A., Bers, D. M., Hell, J. W., Nieves-Cintrón, M., & Navedo, M. F. (2022). Spatiotemporal control of vascular $Ca_V1.2$ by $\alpha 1_C$ S1928 phosphorylation. *Circulation Research*, **131**(12), 1018–1033.

McHugh, B. J., Buttery, R., Lad, Y., Banks, S., Haslett, C., & Sethi, T. (2010). Integrin activation by Fam38A uses a novel mechanism of R-ras targeting to the endoplasmic reticulum. *Journal of Cell Science*, **123**(Pt 1), 51–61.

McHugh, B. J., Murdoch, A., Haslett, C., & Sethi, T. (2012). Loss of the integrin-activating transmembrane protein Fam38A (Piezo1) promotes a switch to a reduced integrin-dependent mode of cell migration. *PLOS ONE*, **7**(7), e40346.

Mercado-Perez, A., & Beyder, A. (2022). Gut feelings: Mechanosensing in the gastrointestinal tract. *Nature Reviews Gastroenterology & Hepatology*, **19**(5), 283–296.

Meredith, A. L., Wiler, S. W., Miller, B. H., Takahashi, J. S., Fodor, A. A., Ruby, N. F., & Aldrich, R. W. (2006). BK calcium-activated potassium channels regulate circadian behavioral rhythms and pacemaker output. *Nature Neuroscience*, **9**(8), 1041–1049.

Nelson, M. T., Cheng, H., Rubart, M., Santana, L. F., Bonev, A. D., Knot, H. J., & Lederer, W. J. (1995). Relaxation of arterial smooth muscle by calcium sparks. *Science*, **270**(5236), 633–637.

Plüger, S., Faulhaber, J., Fürstenau, M., Löhn, M., Waldschütz, R., Gollasch, M., Haller, H., Luft, F. C., Ehmke, H., & Pongs, O. (2000). Mice with disrupted BK channel beta1 subunit gene feature abnormal Ca^{2+} spark/STOC coupling and elevated blood pressure. *Circulation Research*, **87**(11), E53–E60.

Pritchard, H. A. T., Griffin, C. S., Yamasaki, E., Thakore, P., Lane, C., Greenstein, A. S., & Earley, S. (2019). Nanoscale coupling of junctophilin-2 and ryanodine receptors regulates vascular smooth muscle cell contractility. *Proceedings of the National Academy of Sciences of the United States of America*, **116**(43), 21874–21881.

Qiao, M., Penttinen, R., Coli, A., Murciano, N., Maurer, F. M., Wagner, C., Rotordam, M. G., & Kaestner, L. (2025). Piezo1 Channel activators Yoda1 and Yoda2 in the context of red blood cells. *Biomolecules*, **15**(8), 1110.

Ranade, S. S., Qiu, Z., Woo, S. H., Hur, S. S., Murthy, S. E., Cahalan, S. M., Xu, J., Mathur, J., Bandell, M., Coste, B., Li, Y. S., Chien, S., & Patapoutian, A. (2014). Piezo1, a mechanically activated ion channel, is required for vascular development in mice. *Proceedings of the National Academy of Sciences of the United States of America*, **111**(28), 10347–10352.

Ren, J., Xin, F., Liu, P., Zhao, H. Y., Zhang, S. T., Han, P., Huang, H. X., & Wang, W. (2016). Role of BK(Ca) in stretch-induced relaxation of colonic smooth muscle. *Biomed Research International*, **2016**, 9497041.

Ríos, E. (2018). Calcium-induced release of calcium in muscle: 50 years of work and the emerging consensus. *Journal of General Physiology*, **150**, 521–537.

Rousseau, E., Smith, J. S., & Meissner, G. (1987). Ryanodine modifies conductance and gating behavior of single Ca2+ release channel. *American Journal of Physiology*, **253**(3 Pt 1), C364–C368.

Sanders, K. M. (2008). Regulation of smooth muscle excitation and contraction. *Neurogastroenterology & Motility*, **20**(suppl 1), 39–53.

Sanders, K. M. (2019). Spontaneous electrical activity and rhythmicity in gastrointestinal smooth muscles. *Advances in Experimental Medicine and Biology*, **1124**, 3–46.

Sanders, K. M., Drumm, B. T., Cobine, C. A., & Baker, S. A. (2023). Ca^{2+} dynamics in interstitial cells: Foundational mechanisms for the motor patterns in the gastrointestinal tract. *Physiological Reviews*, **104**(1), 329–398.

Sanders, K. M., & Don Koh, S. (2006). Two-pore-domain potassium channels in smooth muscles: New components of myogenic regulation. *The Journal of Physiology*, **570**(1), 37–43.

Sanders, K. M., Koh, S. D., Ro, S., & Ward, S. M. (2012). Regulation of gastrointestinal motility–insights from smooth muscle biology. *Nature Reviews Gastroenterology & Hepatology*, **9**(11), 633–645.

Santana, L. F., Cheng, H., Gómez, A. M., Cannell, M. B., & Lederer, W. J. (1996). Relation between the sarcolemmal Ca^{2+} current and Ca^{2+} sparks and local control theories for cardiac excitation-contraction coupling. *Circulation Research*, **78**(1), 166–171.

Santana Nunez, D, Malik, A. B., Lee, Q., Ahn, S. J., Coctecon-Murillo, A., Lazarko, D., Levitan, I., Mehta, D., & Komarova, Y. A. (2023). Piezo1 induces endothelial responses to shear stress via soluble adenylyl cyclase-IP_3R2 circuit. *iScience*, **26**(5), 106661.

Shen, Z., Gelashvili, Z., & Niethammer, P. (2026). Endoplasmic reticulum disruption stimulates nuclear membrane mechanotransduction. *Nature Cell Biology*, **28**(1), 125–134.

Smith, K. A., Chuntharpursat-Bon, E., Povstyan, O. V., Debant, M., Kinsella, J. A., Revill, C., Fagnen, C., Shi, J., Foster, R., Beech, D. J., & Kalli, A. C. (2025). Regulation of PIEZO1 channel force sensitivity by interblade handshaking. *Science Advances*, **11**(24), eadt7046.

Takeda, Y., Nystoriak, M. A., Nieves-Cintrón, M., Santana, L. F., & Navedo, M. F. (2011). Relationship between Ca2+ sparklets and sarcoplasmic reticulum Ca^{2+} load and release in rat cerebral arterial smooth muscle. *American Journal of Physiology-Heart and Circulatory Physiology*, **301**(6), H2285–H2294.

Townson, J., & Progida, C. (2025). The emerging roles of the endoplasmic reticulum in mechanosensing and mechanotransduction. *Journal of Cell Science*, **138**(4), jcs263503.

Vasileva, V. Y., Sudarikova, A. V., & Chubinskiy-Nadezhdin, V. I. (2025). Functional coupling of Piezo1 channels and Ca^{2+}-activated ion channels in the plasma membrane: Fine-tunable interplay with wide-range signaling effects. *American Journal of Physiology-Cell Physiology*, **328**(4), C1338–C1345.

Wang, W., Huang, H., Hou, D., Liu, P., Wei, H., Fu, X., & Niu, W. (2010). Mechanosensitivity of STREX-lacking BKCa channels in the colonic smooth muscle of the mouse. *American Journal of Physiology Gastrointestinal and Liver Physiology*, **299**(6), G1231–G1240.

Wang, Y., Chi, S., Guo, H., Li, G., Wang, L., Zhao, Q., Rao, Y., Zu, L., He, W., & Xiao, B. (2018). A lever-like transduction pathway for long-distance chemical- and mechano-gating of the mechanosensitive Piezo1 channel. *Nature Communications*, **9**(1), 1300.

Won, K.-J., Sanders, K. M., & Ward, S. M. (2005). Interstitial cells of Cajal mediate mechanosensitive responses in the stomach. *Proceedings of the National Academy of Sciences of the United States of America*, **102**(41), 14913–14918.

Yang, Y., Valencia, L. A., Lu, C.-H., Nakamoto, M. L., Tsai, C.-T., Liu, C., Yang, H., Zhang, W., Jahed, Z., Lee, W.-R., Santoro, F., Liou, J., Wu, J. C., & Cui, B. (2024). Plasma membrane curvature regulates the formation of contacts with the endoplasmic reticulum. *Nature Cell Biology*, **26**(11), 1878–1891.

Zechini, L., Camilleri-Brennan, J., Walsh, J., Beaven, R., Moran, O., Hartley, P. S., Diaz, M., & Denholm, B. (2022). Piezo buffers mechanical stress via modulation of intracellular Ca^{2+} handling in the *Drosophila* heart. *Frontiers in Physiology*, **13**, 1003999.

Zhang, T., Chi, S., Jiang, F., Zhao, Q., & Xiao, B. (2017). A protein interaction mechanism for suppressing the mechanosensitive Piezo channels. *Nature Communications*, **8**(1), 1797.

Zhou, Y., & Lingle, C. J. (2014). Paxilline inhibits BK channels by an almost exclusively closed-channel block mechanism. *Journal of General Physiology*, **144**(5), 415–440.

Additional information

Data availability statement

All data supporting the findings of this study are available within the manuscript and its Appendix materials. For experiments with sample sizes $n \leq 30$ individual data points are plotted in the figures. Source data are deposited at Zenodo (https://doi.org/10.5281/zenodo.21601483), and the custom Python-based wire myography analysis toolkit is publicly available at https://doi.org/10.5281/zenodo.18472624.

Competing interests

The authors declare no competing interests.

Author contributions

Conceptualization: G.M.B., L.F.S., S.A.B. and M.F.N. Methodology: G.M.B., S.A.B., M.F.N., L.F.S., D.M. and N.D.R. Software: G.M.B. Validation: G.M.B., M.A.M.B., E.C.L. and D.M. Formal analysis: G.M.B., D.M., E.C.L. and S.I.U. Investigation: G.M.B., D.M., E.C.L., S.I.U., C.M., J.P.T., M.A.M.B. and N.D.R. Resources: S.J.M., S.A.B., M.F.N. and

L.F.S. Data curation: G.M.B. Writing – original draft: G.M.B. Writing – review and editing: all authors. Visualization: G.M.B., J.P.T., E.C.L., S.I.U. and D.M. Supervision: G.M.B., M.F.N., L.F.S., S.J.M. and D.M. Project administration: G.M.B. Funding acquisition: G.M.B., S.J.M., M.F.N. and L.F.S.

All authors approved the final version of the manuscript and agreed to be accountable for all aspects of the work in ensuring that questions related to the accuracy or integrity of any part of the work are appropriately investigated and resolved. All persons designated as authors qualify for authorship, and all those who qualify for authorship are listed.

Funding

This work was supported by the National Institutes of Health Grants: K08DK143334 (G.M.B.), KL2TR001859 (G.M.B.), R01HL168874 (L.F.S.), R01HL180444 (M.F.N.), R01DK125415 (S.J.M.), R01DK140012 (S.J.M.); the American Heart Association: 26POST1550945 (D.M.) and the Hartwell Foundation: A252454 (G.M.B.).

Acknowledgements

We sincerely thank Brandon Light, Michele Persiani, Camryn Sellers-Porter, Jessica Santana and Trinity Chow from the Immature Gut Biology Lab for their vital technical help and operational support. We also greatly appreciate Rosie Dixon, Madeline Nieves-Cintron and Paula Rhana for their insightful discussions and valuable suggestions that significantly influenced the development of this work.

Generative AI statement

During the preparation of this manuscript the authors used Claude (Anthropic; Claude Opus 4.6-4.8) for two purposes: (1) to edit and refine author-written text for clarity, flow, readability and consistent formatting; and (2) to assist in writing Python code that extracted contractile parameters from wire myography recordings, a measurement normally performed manually using LabChart. The automated output was validated against manual analysis of the same recordings, and the two were confirmed to agree before any values were used. No figures or graphical elements were generated using AI; all graphs were prepared using GraphPad Prism. The tool was not used to generate scientific claims or interpretations nor to collect data. The authors reviewed, tested and verified all AI-assisted code and edited all AI-assisted text and take full responsibility for the accuracy, integrity and content of the manuscript, including all data, analyses, interpretations and references.

Keywords

calcium signalling, GI smooth muscle, mechanotransduction, Piezo1, sarcoplasmic reticulum

Supporting information

Additional supporting information can be found online in the Supporting Information section at the end of the HTML view of the article. Supporting information files available:

Peer Review History